EPJ manuscript No.
(will be inserted by the editor)

Glass models on Bethe lattices

O. Rivoire[1], G. Biroli[2], O. C. Martin[1], and M. Mézard[1]

[1] LPTMS, Université Paris-Sud, Orsay Cedex 91405 France
[2] Service de Physique Théorique CEA-Saclay, Orme des Merisiers - 91191 Gif sur Yvette France

Abstract. We consider "lattice glass models" in which each site can be occupied by at most one particle, and any particle may have at most ℓ occupied nearest neighbors. Using the cavity method for locally tree-like lattices, we derive the phase diagram, with a particular focus on the vitreous phase and the highest packing limit. We also study the energy landscape via the configurational entropy, and discuss different equilibrium glassy phases. Finally, we show that a kinetic freezing, depending on the particular dynamical rules chosen for the model, can prevent the equilibrium glass transitions.

PACS. 64.70.Pf Glass transitions – 64.60.Cn Order-disorder and statistical mechanics of model systems – 75.10.Nr Spin-glass and other random models

1 Introduction

The thermodynamics of vitreous materials is a long standing yet very alive subject of study [1]. In spite of much research, it remains unclear whether this "amorphous" state of matter can exist in equilibrium; even if it cannot, probably the underlying crystalline equilibrium phase is irrelevant for understanding the physics of glassy systems. As experience has shown in other contexts, a lot of understanding can be gained by looking at models simple enough to be analyzed but that retain the essential physics. Following this strategy, several recent works have focused on lattice models for structural glasses.

Lattice gas models with hard core exclusion, i.e., with each site being occupied by at most one particle, designed to reproduce the glass phenomenology, fall into two distinct classes. A first class consists of kinetically constrained models [2] which have a glassy behavior forced by a *dynamical constraint* on allowed moves, but otherwise trivial equilibrium properties. An example is the Kob-Andersen model [3] where a particle is allowed to move only if before and after its move it has no more than some number m neighboring particles. In this case the slow dynamic displays several remarkable properties like for example an avoided transition toward a cooperative "super-Arrhenius" dynamics [4]. Physically, the kinetically constrained models are based on the assumption that the glassy behavior is due to an increasing dynamical correlation length whereas static correlations play no role. Thus, the possibility of a thermodynamic glass transition is excluded from the beginning.

In contrast, the models we will discuss here belong to a second class where the glassy features are generated through a *geometric constraint* on allowed configurations. In this case a thermodynamic equilibrium glass transition independent of the chosen local dynamical rules may exist. Indeed, as we shall show in the following, it takes place for models on a Bethe lattice. Such models were first introduced in Ref. [5] and some variants have been elaborated since then [6, 7].

In this paper, we study the lattice glass models on "Bethe lattices" which are random graphs with a fixed connectivity. This kind of approach provides an approximation scheme for the lattice glasses on Euclidean lattices having the same value of the connectivity, in the same way as the Bethe approximation allows one to compute approximate phase diagrams of non frustrated systems. Furthermore this approximation can be improved systematically, at least in principle, by implementing higher order cluster variational methods. But this random graph study is also interesting for its own sake. In particular we analyze in detail the limit of diverging chemical potential. In this limit, one recovers an optimization problem which is the lattice version of close-packing of spheres, a problem that has challenged mathematicians for many decades [8] and is still matter of debate today [9].

With respect to their Euclidean counterparts, the lattice glasses on Bethe lattices have one important difference: the existence of the random lattice, even with fixed connectivity, forbids crystalline ordering. This loss is also an advantage in that the absence of crystal phases makes it easier to study the glass phase. Indeed, when the density of the system is increased, we find a thermodynamical phase transition from a liquid phase to a glass phase. We can determine the phase diagram analytically, focusing in particular on the liquid to glass transition. In many systems this transition is of the "random first order" [10–13] type, also called "one-step replica symmetry breaking" [14]. On the Bethe lattice there are actually two transitions: when increasing the density or chemical potential, one first finds a dynamical transition in which ergodicity is broken, then

a static phase transition. The intermediate phase is such that the thermodynamic properties are those of the liquid phase, in spite of the ergodicity breakdown. At the static transition the entropy and energy are continuous, with a jump in specific heat. Therefore the Bethe-lattice glass models provide clear solvable examples of a system of interacting particles exhibiting the scenario for the glass transition which was proposed in [10–13] by analogy with some spin glass systems. This scenario is known to be a mean-field one, which does not take into account the nucleation processes that can occur in Euclidean space. It is generally believed that nucleation processes transform the dynamical transition into some cross-over of the dynamics from a fast one to a slow, activated relaxation [10–13, 15]. Whether the static transition survives in realistic system is unknown so far. In this paper we will not discuss the relevance and modifications of the mean field scenario when applied to finite dimensional problems since we have nothing to add to existing speculations. Let us just mention that the lattice glasses provide the best examples on which these issues can be addressed. The first step of such a study is to have a detailed understanding of the mean field theory, and this is what we do in the present paper.

Note that some of the results have appeared in Ref. [5]; here we give a new and extensive discussion on the nature of the different possible equilibrium glassy phases.

On top of the thermodynamic study, we have also studied the dynamical arrest of the lattice glasses on Bethe lattices. The dynamical arrest depends on the specific dynamical rule that is implemented. We show that this dynamical arrest is in general unrelated to the energy landscape transitions found in the thermodynamic approach. In particular, in some models, a dynamical arrest takes place at a density *smaller* than the one of the dynamical glass transition. In kinetically constrained problems, such mean field arrest transitions are known to become crossovers in finite dimensional systems. The corresponding arrest behavior on our lattice glass models is not known yet.

The outline of this paper is as follows. In Sect. 2, we introduce the models on lattices of arbitrary types and define the relevant thermodynamics quantities. In Sect. 3, we address the case of loop-less regular lattices, called Cayley trees when surface sites are included and Bethe lattices when surface effects can be neglected. We show that low densities correspond to a liquid phase described by the Bethe-Peierls approximation, but that inhomogeneous phases must be present at higher densities. However, the strong boundary dependence of models on Cayley trees does not allow one to define such dense phase in the interior. To overcome this problem, we consider instead in Sect. 4 random regular graphs; they share with Cayley trees a local tree-like structure but are free of surface effects and thus provide a natural generalization of Bethe lattices adequate for dense phases. Our study on random graphs is performed by means of the cavity method [16] which predicts for high densities a glassy phase. In Sect. 5, we focus on the close-packing limit and discuss in detail the nature of this glassy phase. Finally in Sect. 6, we comment on the differences between the equilibrium glass transition of our models and the kinetic transitions or dynamical arrests related to specific local dynamical rules. In particular we show that for some models the dynamical arrest takes place *before* the equilibrium glass transition.

2 Lattice Models

2.1 Constraints on local arrangements

When packing spheres in three dimensions, the preferred local ordering is icosahedral; this does not lead to a periodic crystalline structure and is the source of frustration. To model this type of frustration, we forbid certain local arrangements of the particles on the lattice. This can be done using two or n-body interactions. We follow [5] and set the interaction energy to be infinite if a particle has strictly more than ℓ particles as nearest neighbors. The interactions thus act as "geometric" constraints.

Note that these geometric constraints are very similar to the kinetic constraints of the Kob-Andersen model [3]. However, as we shall show, the fact that they are encoded in an energy function makes a big difference physically, in particular for the thermodynamic behavior.

We work in the grand canonical ensemble and introduce a chemical potential. All energies being zero or infinity, temperature plays no role. The thermodynamics for a given system (i.e., a given lattice) is then defined by the grand canonical partition function

$$\Xi(\mu) = \sum_{n_1,\dots,n_N \in \{0,1\}} C_\ell(n_1,\dots,n_N)\; e^{\mu \sum_{i=1}^N n_i}. \qquad (1)$$

The dynamical variables are the site occupation values: $n_i = 0$ if site i is empty and $n_i = 1$ if a particle is on that site. We take all the particles to be identical. In Eq. (1), μ is the chemical potential, and $C_\ell(n_1,\dots,n_N)$ implements all the geometrical constraints: it is the product of local constraints, one for each of the N sites. The term for site i is

$$\theta\left(\ell - n_i \sum_{j \in \mathcal{N}(i)} n_j\right) \qquad (2)$$

where $\mathcal{N}(i)$ denotes the set of neighbors of i, and $\theta(x) = 0$ if $x < 0$, $\theta(x) = 1$ if $x \geq 0$.

For sake of concreteness and simplicity, we will focus in the core of the paper on the $\ell = 1$ case when each particle has at most one neighbor, deferring the general ℓ case to Appendix A. Most numerical results will be given for the "basic model", noted BM, for which $\ell = 1$ and $k = 2$.

2.2 Observables

For a given "lattice" of N sites and type (Euclidean, tree, random graph, ...), and for a given form of constraints

(i.e., a value of ℓ), there is only one parameter, the chemical potential μ. It is useful to introduce the grand potential $\mu\Omega(\mu)$ and its density $\omega(\mu) \equiv \Omega(\mu)/N$, so that

$$\Xi(\mu) = \exp\left[-\mu\Omega(\mu)\right] = \exp\left[-N\mu\omega(\mu)\right]. \qquad (3)$$

The pressure is given by $p = -\mu\omega(\mu)$ and the particle density is

$$\rho(\mu) \equiv \left\langle \frac{\sum_i n_i}{N} \right\rangle = \frac{1}{N\Xi(\mu)} \frac{d\Xi(\mu)}{d\mu} = -\frac{d(\mu\omega)}{d\mu} = \frac{dp(\mu)}{d\mu}. \qquad (4)$$

Clearly, ρ is an increasing function of μ. When $\mu \to -\infty$, the system becomes empty, a typical equilibrium configuration having almost all $n_i = 0$, so $\rho \to 0$. In the opposite limit, $\mu \to +\infty$, there is in effect a strong *penalty* for each vacancy, but the geometrical constraints prevent all sites from being occupied; then ρ has a maximum value strictly less than 1. When $N \to \infty$, this value is expected to converge to a limit ρ_∞. Obviously, ρ_∞ depends on the type of lattice and on the parameter ℓ.

We can define similarly the entropy density $s(\mu)$:

$$s(\mu) \equiv \frac{\ln \Xi(\mu)}{N} - \mu\rho(\mu) = -\mu\omega(\mu) - \mu\rho(\mu) \qquad (5)$$

where again $s(\mu)$ should have a well defined thermodynamic limit.

Other physical quantities that we shall study include susceptibilities associated with two-site connected correlation functions of the type $\langle n_i n_j \rangle_c$. At low densities the n_i have only short range correlations. When μ increases, ρ also increases; then the constraints become more important and correlations grow. When the density is close to ρ_∞, the system will be very "rigid", allowing few fluctuations in the local density. It is plausible that the susceptibility will diverge at some critical value of μ, separating a liquid phase at low μ from a denser phase at large μ.

The nature of this dense phase, and of the transition, will depend on the lattice, on the boundary conditions, and need not be associated with a crystalline order. When it is not crystalline, we want a statistical description of the dominant equilibrium configurations. In particular, if these configurations form clusters, it is of interest to estimate the number of such clusters. We will do this by computing the "configurational entropy" $\Sigma(\rho)$ (also called *complexity*) associated with the number of clusters (also called *states*) of configurations with a given density ρ.

3 Models on Cayley trees

3.1 Iteration equations

We first consider glass models defined on regular *trees*, i.e. connected graphs with no loops and fixed connectivity. We distinguish *rooted trees* where a site called the *root* is connected to only k neighbors while all the other sites (except for those at the surface, that is the leaves of the tree) have $k+1$ neighbors. A *Cayley tree* is obtained by connecting a site to the roots of $k+1$ rooted trees.

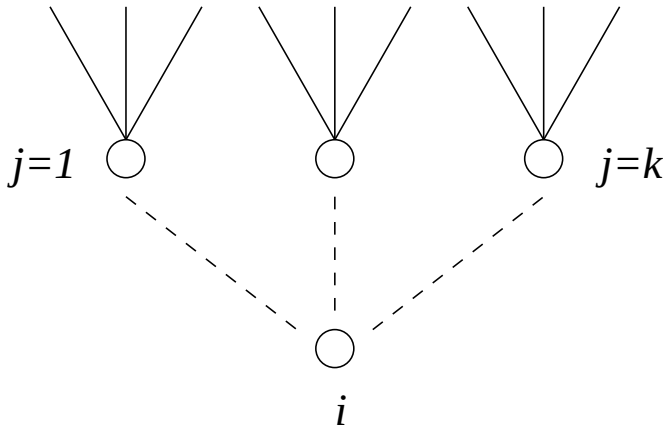

Fig. 1. An iterative method is used to compute the partition function on rooted trees. We begin with k rooted trees with roots $j = 1, \ldots, k$ and form a new rooted tree by joining a site i to each of them. The possible occupations of site i depend on the occupations of the sites $j = 1, \ldots, k$ and on the type of constraint used.

When the graph is a rooted tree, the grand canonical partition function can be computed by recursion starting from the leaves. To do this, we follow conditional partition functions because we need to know how to apply the constraints when joining the sub-trees (cf. Fig. 1). This provides a generalization of the well-known transfer matrix method for one dimensional systems (which can be viewed as rooted trees with $k = 1$).

In our class of constraints, we need to know whether the root sites are occupied, and if they are, whether they have ℓ occupied neighbors or less than that. Let $\Xi_i^{(e)}$, $\Xi_i^{(u)}$ and $\Xi_i^{(s)}$ be the conditional partition functions for a rooted sub-tree i when its root node i is empty (e), occupied but the constraint unsaturated (u) and finally occupied and the constraint saturated (s), i.e., the root site has ℓ neighboring particles. Then the conditional partition functions for the rooted tree obtained by joining the sub-trees are easily computed.

For instance, in the $\ell = 1$ case where each particle can have at most one neighbor, when merging k rooted trees $(j = 1, \ldots k)$ to obtain a new tree rooted say at site i, we have

$$\Xi_i^{(e)} = \prod_{j=1}^{k} \left(\Xi_j^{(e)} + \Xi_j^{(u)} + \Xi_j^{(s)} \right), \qquad (6)$$

$$\Xi_i^{(u)} = e^{\mu} \prod_{j=1}^{k} \Xi_j^{(e)}, \qquad (7)$$

$$\Xi_i^{(s)} = e^{\mu} \sum_{j=1}^{k} \Xi_j^{(u)} \prod_{p \neq j} \Xi_p^{(e)}. \qquad (8)$$

Naturally, the total partition function is the sum of the conditional partition functions.

To study these recursions, it is convenient to consider local fields defined via ratios of conditional partition functions. Here we introduce on a root site i two fields a_i and

b_i defined as

$$e^{-\mu a_i} \equiv \frac{\Xi_i^{(e)}}{\Xi_i^{(e)} + \Xi_i^{(u)} + \Xi_i^{(s)}}, \tag{9}$$

$$e^{-\mu b_i} \equiv \frac{\Xi_i^{(e)}}{\Xi_i^{(e)} + \Xi_i^{(u)}}. \tag{10}$$

The first quantity is the probability for the root of a rooted tree to have an empty site (e); the second is the ratio of that probability and the probability to have a non saturated site. The use of μ when defining these fields is to simplify the analysis at large μ (cf. Sect. 5). These two fields form a closed recursion under the joining of subtrees; for instance when $\ell = 1$,

$$\begin{aligned} a_i &= \hat{a}(a_1, b_1, \dots, a_k, b_k) \\ &= \frac{1}{\mu} \ln \left[1 + e^{\mu(1 - \sum_{j=1}^k a_j)} \left(1 + \sum_{j=1}^k (e^{\mu b_j} - 1) \right) \right], \end{aligned} \tag{11}$$

$$\begin{aligned} b_i &= \hat{b}(a_1, b_1, \dots, a_k, b_k) \\ &= \frac{1}{\mu} \ln \left[1 + e^{\mu(1 - \sum_{j=1}^k a_j)} \right]. \end{aligned} \tag{12}$$

Note that the use of ratios of conditional partition functions leads to recursions for two quantities rather than the initial three. To recover all the information in the initial recursions, we also keep track of the change in the grand potential. If $\Omega_1, \dots \Omega_k$ give the grand potentials of the k sub-trees, we have after the merging

$$\Omega_i = \sum_{j=1}^k \Omega_j + \Delta\hat{\Omega}_{\text{iter}}(a_1, b_1, \dots, a_k, b_k) \tag{13}$$

where $\Delta\hat{\Omega}_{\text{iter}}(a_1, b_1, \dots, a_k, b_k) = \Delta\Omega_{\text{iter}}$ is defined via

$$e^{-\mu \Delta\Omega_{\text{iter}}} = \frac{\Xi_i}{\prod_{j=1}^k \Xi_j} = \frac{\Xi_i^{(e)} + \Xi_i^{(u)} + \Xi_i^{(s)}}{\prod_{j=1}^k \left(\Xi_j^{(e)} + \Xi_j^{(u)} + \Xi_j^{(s)} \right)}. \tag{14}$$

With our definition of the fields, we have then $\Delta\hat{\Omega}_{\text{iter}} = -\hat{a}$. From here on, we shall use the short-hand notation: $h \equiv (a, b)$ and $h_i = \hat{h}(h_1, \dots, h_k)$ with

$$\begin{aligned} &\hat{h}\left(h_1 = (a_1, b_1), \dots, h_k = (a_k, b_k)\right) = \\ &\left(\hat{a}(a_1, b_1, \dots, a_k, b_k), \hat{b}(a_1, b_1, \dots, a_k, b_k) \right). \end{aligned} \tag{15}$$

3.2 Liquid phase

Begin now on the leaves of a rooted tree, assuming that some kind of boundary condition is specified there. For example, the n_i could be fixed, or their probability distribution could be given. These determine the initial values of the conditional partition functions and thus of the fields. We iterate the recursions, propagating the fields away from the leaves by performing mergings. When $\mu \ll -1$, these iterations are contracting and so the fields converge to a value that is independent of the starting values on the leaves. The distribution of fields in the bulk (away from the leaves) is then given by

$$\mathcal{P}(h) = \delta(h - h_{\text{liq}}) \tag{16}$$

with the fixed point condition $h_{\text{liq}} = \hat{h}(h_{\text{liq}}, \dots, h_{\text{liq}})$. We determine the fixed point for all μ, and refer to it as the *liquid* solution; its physical relevance includes at least the region $\mu \ll -1$.

We can now merge consistently $k+1$ rooted trees to obtain a Cayley tree. We then have a liquid (or paramagnetic) phase, all correlations being short range and the heart of the Cayley tree being insensitive to the boundary conditions, even though a finite fraction of the sites live on the surface. In this regime, the homogeneous interior of the Cayley tree can be used to define the *Bethe lattice model*.

In this context, also known as the *Bethe-Peierls approximation*, the density ω can be obtained from the following construction. Start with $(k+1)$ Bethe lattices; for each of them, pick an edge and remove it, leading to $2(k+1)$ infinite rooted trees. Then form *two* Bethe lattices by adding two sites and connecting each to $(k+1)$ of the rooted trees. Now the difference in grand potential between the resulting two Bethe lattices and the initial ones is just twice the grand potential per site (since two sites were added) and can be written as

$$2\omega = -(k+1)\Delta\Omega_{\text{edge}} + 2\Delta\Omega_{\text{site}} \tag{17}$$

where $\Delta\Omega_{\text{edge}}$ is the difference in grand potential corresponding to adding an edge and $\Delta\Omega_{\text{site}}$ to merging $(k+1)$ branches into a new site. Such quantities are easily expressed with the partition functions of rooted trees; for instance for $\ell = 1$ we obtain

$$\begin{aligned} &e^{-\mu \Delta\hat{\Omega}_{\text{site}}(a_1, b_1, \dots, a_{k+1}, b_{k+1})} \\ &= 1 + e^{\mu(1 - \sum_{j=1}^{k+1} a_j)} \left(1 + \sum_{j=1}^{k+1} (e^{\mu b_j} - 1) \right) \end{aligned} \tag{18}$$

and similarly

$$\begin{aligned} &e^{-\mu \Delta\hat{\Omega}_{\text{edge}}(a_1, b_1, a_2, b_2)} \\ &= \left[\Xi_1^{(e)} \Xi_2^{(e)} + \Xi_1^{(e)} \left(\Xi_2^{(u)} + \Xi_2^{(s)} \right) + \left(\Xi_1^{(u)} + \Xi_1^{(s)} \right) \Xi_2^{(e)} \right. \\ &\quad \left. + \Xi_1^{(u)} \Xi_2^{(u)} \right] \Big/ (\Xi_1 \Xi_2) \\ &= e^{-\mu(a_1 + a_2)} \left(e^{\mu a_1} + e^{\mu a_2} + e^{\mu(b_1 + b_2)} - e^{\mu b_1} - e^{\mu b_2} \right). \end{aligned} \tag{19}$$

Note that we have the simple relation

$$\begin{aligned} \Delta\hat{\Omega}_{\text{site}}(h_1, \dots, h_{k+1}) =& \Delta\hat{\Omega}_{\text{iter}}(h_1, \dots, h_k) \\ &+ \Delta\hat{\Omega}_{\text{edge}} \left(\hat{h}(h_1, \dots, h_k), h_{k+1} \right) \end{aligned} \tag{20}$$

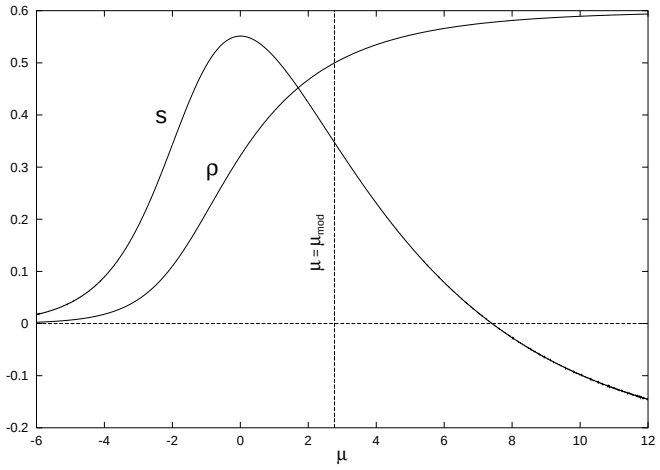

Fig. 2. μ dependence of the particle density ρ and entropy s of the liquid phase for the BM ($\ell = 1$, $k = 2$). The failure of the liquid phase to correctly describe the model at high μ is evidenced by the negative sign of the entropy for $\mu > \mu_{s=0} \simeq 7.40$. But in fact the liquid solution becomes linearly unstable well before, at $\mu_{\rm mod} \simeq 2.77$ (vertical line).

whose interpretation is clear: the addition of one site by merging $k+1$ rooted trees $\mathcal{T}_1, \dots, \mathcal{T}_{k+1}$ can be decomposed into the construction of a new rooted tree $\mathcal{T}_0$ obtained by merging a site to the k rooted trees $\mathcal{T}_1, \dots, \mathcal{T}_k$ and the addition of an edge between $\mathcal{T}_0$ and $\mathcal{T}_{k+1}$. Moreover $\Delta\hat{\Omega}_{\rm site}$ is obtained from $\Delta\hat{\Omega}_{\rm iter}$ by making the substitution $k \to k+1$. The expressions (18-19) are written for the general inhomogeneous case but simplify in the liquid phase where all the fields take their liquid value.

In Fig. 2, we show as illustration the liquid's density ρ and its entropy density s, as a function of μ for the BM. Since the models are discrete, the equilibrium entropy should never go negative. Nevertheless, the liquid solution at large μ, $\mu > \mu_{s=0}$, leads to $s_{\rm liq} < 0$ except in very special cases such as $k = 1$. Thus there must exist a phase transition at $\mu_c \leq \mu_{s=0}$, and the liquid phase cannot be the equilibrium phase at $\mu > \mu_c$. Clearly, one must determine when the liquid solution is physically relevant; when it is not, one should find other solutions [5].

3.3 Linear stability limit of the liquid

The Bethe-Peierls approximation fails when the bulk properties of the Cayley tree become sensitive to the boundary conditions. This "instability" may show up via a loss of stability of the fixed point equations as given by a simple linear analysis. Indeed, starting with fields identically and independently distributed on the leaves, the field distribution $\mathcal{P}_{g+1}(h)$ at "generation" $g+1$ is related to that at generation g by

$$\mathcal{P}_{g+1}(h_i) = \int \prod_{j=1}^{k} dh_j \mathcal{P}_g(h_j) \delta\left(h_i - \hat{h}(h_1, \dots, h_k)\right). \tag{21}$$

Close to a liquid solution we have to first order

$$\langle \delta h \rangle_{g+1} = k \left. \frac{\partial \hat{h}}{\partial h_1} \right|_{\rm liq} \langle \delta h \rangle_g \tag{22}$$

where $\delta h \equiv h - h_{\rm liq}$ and $\langle . \rangle_g$ refers to the average using the distribution $\mathcal{P}_g$. Since h is a two-component vector, $\partial\hat{h}/\partial h_1$ is actually a 2×2 Jacobian matrix. If λ_1 denotes the eigenvalue of largest modulus of that matrix, the stability criterion simply reads

$$k|\lambda_1| \leq 1. \tag{23}$$

When $k|\lambda_1| > 1$, the liquid solution is unstable to perturbations homogeneous within a generation; we shall refer to it as the *modulation instability* because it is a transition to a regime with successive (homogeneous) generations carrying different fields.

An alternative point of view consists in studying response functions. At finite μ, the response to a perturbation is related to correlations through the fluctuation-dissipation theorem, and an instability can be detected by means of a diverging susceptibility. Thus, we recover the previous result by computing the *linear susceptibility* in the liquid phase, looking for the point where it becomes infinite. The linear susceptibility is defined in terms of connected correlation functions $\langle n_i n_j \rangle_c$ via

$$\chi_1(\mu) \equiv \frac{d\rho}{d\mu} = \frac{1}{N} \sum_{i,j} \langle n_i n_j \rangle_c. \tag{24}$$

Making use of the homogeneity of the liquid solution, it can be rewritten

$$\chi_1(\mu) = \rho(1-\rho) + \sum_{r=1}^{\infty} (k+1) k^{r-1} \langle n_0 n_r \rangle_c \tag{25}$$

where n_0 and n_r are taken at distance r in the tree. The series converges provided that

$$\ln k + \lim_{r \to \infty} \frac{\ln \langle n_0 n_r \rangle_c}{r} < 0. \tag{26}$$

To evaluate $\langle n_0 n_r \rangle_c$, we invoke the fluctuation-dissipation relation

$$\langle n_0 n_r \rangle_c = \frac{\partial \langle n_r \rangle}{\partial h_0^{(c)}} \tag{27}$$

where $h_0^{(c)}$ denotes the external field conjugate to n_0. Since $h_0^{(c)}$ is a function of (the components of) h_0 only, we can use the chain rule

$$\frac{\partial \langle n_r \rangle}{\partial h_0^{(c)}} = \frac{\partial \langle n_r \rangle}{\partial h_{r-1}} \left(\prod_{l=1}^{r-1} \frac{\partial h_l}{\partial h_{l-1}} \right) \frac{\partial h_0}{\partial h_0^{(c)}} \tag{28}$$

where we introduced $h_l \equiv \hat{h}(h_{l-1}, h_{\rm liq} \dots, h_{\rm liq})$ as intermediate fields. In the liquid phase, all these fields are equal and the previous equation factorizes, leading again to $k|\lambda_1| \leq 1$. For instance for the BM, the modulation instability shows up at $\mu_{\rm mod} = 4 \ln 2 \simeq 2.77$, well before the entropy becomes negative at $\mu_{s=0} \simeq 7.40$ as shown in Fig. 2.

3.4 Crystal phase

We can ask whether it is possible to choose boundary conditions such that the interior of the Cayley tree has a periodic structure (for a general tree, the boundary conditions will vary from leaf to leaf). In the $\mu \to \infty$ limit, we expect a crystalline phase to exist whose structure can be easily displayed by starting at the center of the Cayley tree, filling the sites with particles whenever possible. In this case, for the BM, the field $h = (a, b)$ takes three different values h_e, h_u and h_s such that

$$\begin{aligned} h_e &= \hat{h}(h_s, h_s), \\ h_u &= \hat{h}(h_e, h_e), \\ h_s &= \hat{h}(h_e, h_u), \end{aligned} \tag{29}$$

with $h_e = (0, 0)$, $h_u = (1, 1)$ and $h_s = (1, 0)$. The integer values 0 and 1 of the components of these fields reflect the fact that a given site is certainly empty, unsaturated or saturated. For finite μ, fluctuations are present but we can still look for a fixed point of Eq. (29), with $h_e, h_u, h_s \in \mathbb{R}$.

Such a solution, distinct from the liquid one, is found to exist and to be stable for $\mu \geq \mu_{ms}$ with $\mu_{ms} \simeq 2.89$ (ms for *melting spinodal*). Next we want to evaluate the grand potential of this crystalline solution in the bulk. To do so, we first consider the $\mu = \infty$ limit and estimate the density of empty and occupied sites, $\rho_0 = 2/5$ and $\rho_1 = 3/5$, and also the proportion of edges connected to one and two particles, $\pi_1 = 4/5$ and $\pi_2 = 1/5$. Then the crystalline potential can be written as $\omega_{\text{cryst}} = \omega_{\text{site}} - 3/2\ \omega_{\text{edge}}$, with

$$\begin{aligned} \omega_{\text{site}} &= \rho_0 \Delta\hat{\Omega}_{\text{site}}(h_s, h_s, h_s) + \rho_1 \Delta\hat{\Omega}_{\text{site}}(h_u, h_e, h_e), \\ \omega_{\text{edge}} &= \pi_1 \Delta\hat{\Omega}_{\text{edge}}(h_e, h_s) + \pi_2 \Delta\hat{\Omega}_{\text{edge}}(h_u, h_u). \end{aligned} \tag{30}$$

Now for $\mu_{ms} < \mu < \infty$, the structure of the crystal is preserved, with empty and occupied sites being replaced by *most probably* empty or occupied site. Therefore we resort to Eq. (30), using the adequate values of the fields h_e, h_u, h_u, and we keep the same factors $\rho_{0,1}$ and $\pi_{0,1}$. This leads to a melting transition (where $\omega_{\text{liq}} = \omega_{\text{cryst}}$) at $\mu_m \simeq 3.24$.

Comparing $\mu_{ms} \simeq 2.89$ with the location of the liquid's instability $\mu_{\text{mod}} \simeq 2.77$, we have an interval $\mu_{\text{mod}} < \mu < \mu_{ms}$ where no homogeneous nor periodic solution seems to exist. This is to be contrasted with the phase diagram of the hard sphere model studied by Runnels [17] where the presence of a particle on a site forbids the occupation of any of its neighboring sites. That model has been reconsidered recently in two dimensions as a combinatorial problem of counting binary matrices with no two adjacent 1's when $\mu = 0$ [18] and on random graphs as an optimization problem called *vertex cover problem* when $\mu = \infty$ [19]; from the point of view of our lattice glasses, these models correspond to the $\ell = 0$ constraint. In this case the modulation instability coincides exactly with the melting transition (and with the spinodal point), $\mu_m = \mu_{ms} = \mu_{\text{mod}}$. This is due to the special structure of the crystal, organized in alternate shells of empty and occupied sites, and therefore described by a cyclic solution of the liquid equation, $h_1 = \hat{h}(h_0, \ldots, h_0)$ and $h_0 = \hat{h}(h_1, \ldots, h_1)$ with homogeneous shells (i.e., the arguments of $\hat{h}$ are all identical). For $\ell = 1$ no such cyclic solution was found and homogeneous boundary conditions on the leaves yield an *aperiodic* behavior of the recursion $h_{j+1} = \hat{h}(h_j, \ldots, h_j)$. This feature is very specific to the unphysical nature of pure Cayley trees: it does not survive in the random regular graphs which we use below. Therefore we have not pushed its study any further.

4 Models on random regular graphs

4.1 From Cayley trees to random regular graphs

When the Bethe-Peierls approximation no longer holds on a Cayley tree, the sensitivity to boundary conditions does not allow one to define a thermodynamic limit and therefore may lead to unphysical results. Since that is due to the presence of a finite fraction of the sites on the surface, one way to get rid of this problem is to define Bethe lattice models as models on *random regular graphs*. These are simple graphs with fixed connectivity $k + 1$, *simple* meaning that they have no trivial loops (joining a site to itself) and no multi-edges (no two edges join the same sites). Here we will use the cavity method to obtain results for a typical random graph (chosen uniformly in the set of all random regular graphs with a fixed connectivity $k + 1$).

When the number N of sites is large, typical random regular graphs look locally like trees, having only long loops of order $\ln N$. Therefore the recursive equations still (locally) hold, making these lattices analytically tractable. The large loops implement an analog of generic boundary conditions and the resulting frustration forbids crystalline orderings. One then expects the system to possess an equilibrium glass phase in the high μ region.

In the low μ phase, the liquid solution is recovered. The corresponding Bethe-Peierls approximation is called the *factorized replica symmetric approximation* in the context of the cavity method where the vocabulary is inherited from the treatment of spin glasses based on the replica trick. However the glassy high μ regime will be characterized by the existence of many solutions of the local equations and we will have to resort to the replica symmetry breaking (rsb) formalism to correctly take into account the specific organization of these solutions [20].

4.2 Entropy crisis

Reconsidering the stability of the liquid with the modulation instability now being excluded, we can look for a "spin-glass" instability, to borrow the terminology from magnetic systems where the modulation instability is referred to as the "ferromagnetic instability". This new instability manifests itself as a divergence of the *non-linear susceptibility*, which is defined as

$$\chi_2(\mu) \equiv \frac{1}{N} \sum_{i,j} \langle n_i n_j \rangle_c^2. \tag{31}$$

In the formalism of Sect. 3.3, the instability appears as a widening of the variance $\langle(\delta h)^2\rangle_g$ under the recursion of Eq. (21). Both approaches are equivalent and lead to a stability criterion

$$k|\lambda_1|^2 \leq 1. \tag{32}$$

The eigenvalue λ_1 is the same as for the linear susceptibility since the transfer matrix is just the square of the Jacobian matrix we had in Eq. (22). Note that this condition is always weaker than that for the modulation instability, $k|\lambda_1| \leq 1$. However it is the relevant one in the case of random graphs where homogeneous perturbations are generically incompatible with frustration. If the liquid is locally stable for all μ, a continuous phase transition is excluded. For $\ell = 1$ this happens for $k = 2, 3$ because $\sqrt{k}|\lambda_1(\mu)| < 1$ for all μ with only asymptotically $\sqrt{k}|\lambda_1(\mu)| \to 1$ as $\mu \to \infty$. In the general case, as soon as $\mu_g > \mu_{s=0}$, where μ_g (g for *glass*) is defined by

$$\sqrt{k}|\lambda_1(\mu = \mu_g)| = 1, \tag{33}$$

the resolution of the entropy crisis requires a phase transition before the spin-glass local instability is reached, and we conclude that a *discontinuous* phase transition must take place at $\mu_c \leq \mu_{s=0}$. In that case we expect a behavior similar to that of infinite-connectivity models solved within a one-step replica symmetry breaking (1-rsb) Ansatz, like e.g. the p-spin models ($p > 2$). When $\mu_g < \mu_{s=0}$, as is found for $\ell = 1$ and $k \geq 4$, we can either have a continuous transition at μ_g or a discontinuous transition at $\mu_c < \mu_g$; a study of the *local* stability of the liquid solution says nothing about which case arises.

4.3 Cavity equations

The solution by the cavity method predicts results for quantities averaged over all random regular graphs with size $N \to \infty$, but the problem is more clearly stated on a given finite regular graph. Indeed, we want to solve self-consistently a set of $(k+1)N$ coupled equations for the cavity fields

$$\begin{aligned} &h_{i\to j_0} = \hat{h}(h_{j_1\to i}, \ldots, h_{j_k\to i}) \\ &\forall i \quad \forall \{j_0, j_1, \ldots, j_k\} \in \mathcal{N}(i) \end{aligned} \tag{34}$$

where $\mathcal{N}(i)$ denotes the set of $k+1$ neighbors of i. Thus for each $i \in \{1, \ldots, N\}$ we have $k+1$ equations corresponding to the different choices of $j_0 \in \mathcal{N}(i)$. The notation $h_{i\to j}$ refers to the local field on i when the edge to the site j is removed, and it is called a *cavity field*; for a Cayley tree, it corresponds to the field on the root i of a rooted tree obtained when the edge ij has been removed. These local equations are known as the TAP equations in statistical physics [14] and as the belief propagation equations in computer science [21]. The contact between both points of view has recently lead to establish that these equations must always have at least one fixed point corresponding to the minimum of a correctly defined Bethe-Peierls approximated free energy [22]. Their solutions should correspond to the fuzzy concept of *states* ubiquitous in the spin-glass literature.

A message passing algorithm can be used to try to solve these equations on a given graph of large but finite size N. First on each oriented edge we associate local fields $h_{i\to j}$ randomly initialized. Then we proceed iteratively: at each step, all the oriented edges are successively chosen in a random order, and the field on the chosen oriented edge is updated by taking into account the values of its neighbors as prescribed by Eq. (34). The iteration is stopped when a sweep of all the oriented edges results in no change; in such a case we lie at a fixed point of the local equations. However the algorithm may also not converge, in which case no conclusion can be drawn. In practice, we find a rapid convergence toward the liquid solution for $\mu < \mu_{bp}$ and then a failure to converge for $\mu > \mu_{bp}$. The critical μ_{bp} depends slightly on the graph but for large N and large k, it is given by the glass instability, i.e., $\mu_{bp} \to \mu_g$ as $k \to \infty$. In some case (for not too big graphs), we could find a convergence towards a non-liquid distribution, suggesting that the high μ region corresponds in fact to a glassy phase. In order to deal with this phase where the Bethe-Peierls approximation breaks down and simple message passing algorithms fail, we will now introduce the cavity method which provides both an alternative approximation for infinite graphs and insights into elaborating more efficient algorithms for finite graphs [16]. In Appendix D we present an alternative approach based on the replica method.

4.4 One-step replica symmetry breaking cavity method

The local equations Eq. (34) can be written for arbitrary graphs but they provide exact marginal probability distribution (and thus exact particle densities) only for trees. In addition, they are in general intractable. However, they are particularly suited for very large random graphs, where due to the local tree-like structure, they are expected to provide good approximations of the marginals and where additional hypotheses allow for an analytical treatment. To do so, we do not try to find one solution but instead turn to a statistical treatment of sets of solutions.

Being interested in the case where many solutions exist, we fix a μ for which this is supposed to happen. We make the further hypothesis that exponentially many (in N) solutions exist. More precisely, we assume that the number $\mathcal{N}_N(\omega)$ of solutions with a given potential density ω on graphs of size N is given by

$$\mathcal{N}_N(\omega) \sim \exp[N\Sigma(\omega)] \tag{35}$$

where $\Sigma(\omega) \geq 0$ is called the *configurational entropy* (or *complexity*) and is supposed to be an increasing and concave function of the grand potential ω. This is a strong hypothesis which is justified by its self-consistency and by its consequences (in particular it matches with the output of replica theory calculations, cf. Appendix D).

Starting with a graph $\mathcal{G}$, we pick a site i and one of its neighbors $j_0 \in \mathcal{N}(i)$, and define the graph $\mathcal{G}_{i\to j_0}$ as

the connected graph containing i obtained by removing the edge ij_0 from $\mathcal{G}$. If $\mathcal{G}$ is a Cayley tree, $\mathcal{G}_{i\to j_0}$ is nothing but a rooted tree, the appropriate structure to write down recursive relations. We introduce $R_{i\to j_0}(h,\omega)$, the joint probability density, when a solution α of Eq. (34) defined on $\mathcal{G}_{i\to j_0}$ is chosen randomly, that the cavity fields $h^{(\alpha)}_{i\to j_0}$ on i take the value h and the grand potential density $\omega^{(\alpha)}_{i\to j_0}$ the value ω,

$$R_{i\to j_0}(h,\omega) = \frac{1}{N_{\rm sol}}\sum_{\alpha}\delta\left(h-h^{(\alpha)}_{i\to j_0}\right)\delta\left(\omega-\omega^{(\alpha)}_{i\to j_0}\right). \tag{36}$$

The next crucial hypothesis is based on the locally tree-like structure of large random graphs. Indeed, if the graph $\mathcal{G}_{i\to j_0}$ is a rooted tree, the sub-rooted trees $\mathcal{G}_{j_1\to i},\dots,\mathcal{G}_{j_k\to i}$ with $\{j_1,\dots,j_k\}\in\mathcal{N}(i)$ are disjoint and the cavity fields $h_{j_1\to i},\dots,h_{j_k\to i}$ are therefore solutions of uncoupled local equations. In such a case the joint probability distribution factorizes over the independent variables

$$\begin{aligned}&R(h_{j_1\to i},\omega_{j_1\to i};\dots;h_{j_k\to i},\omega_{j_k\to i})\\&= R_{j_1\to i}(h_{j_1\to i},\omega_{j_1\to i})\dots R_{j_k\to i},(h_{j_k\to i},\omega_{j_k\to i})\,.\end{aligned} \tag{37}$$

In addition, a simple relation between the distribution $R_{i\to j_0}$ on a rooted tree $\mathcal{G}_{i\to j_0}$ and the $R_{j_1\to i},\dots,R_{j_k\to i}$ on its sub-rooted trees $\mathcal{G}_{j_i\to i},\dots,\mathcal{G}_{j_k\to i}$ can be written:

$$\begin{aligned}R_{i\to j_0}(h,\omega) = &\int\prod_{r=1}^{k}dh_{j_r}d\omega_{j_r}R_{j_r\to i}(h_{j_r},\omega_{j_r})\\&\delta\left(h-\hat{h}(\{h_{j_r}\})\right)\delta\left[\omega-\frac{1}{N}\left(\sum_{r=1}^{k}N_{j_r}\omega_{j_r}+\Delta\hat{\Omega}_{\rm iter}(\{h_{j_r}\})\right)\right]\end{aligned} \tag{38}$$

where the N_{j_r} are the sizes of the sub-trees and $N=\sum_r N_{j_r}+1$ is the size of $\mathcal{G}_{i\to j_0}$. A further simplification takes place on regular trees where, due to the absence of local quenched disorder, the equations for $h_{j_1\to i},\dots,h_{j_k\to i}$ are identical. In such a case, $R_{i\to j_0}$ is in fact independent of the oriented edge $i\to j_0$. For a large random regular graph, we assume that the same properties hold. Note that the last hypothesis, yielding $R_{i\to j_0}=R$ is called the *factorization* approximation and could be relaxed by working with a distribution $\mathcal{R}[R]$ of the R over the various edges [20]. However the factorization approximation should be exact on random regular graph for systems without disorder provided that no spontaneous breaking of "translational" invariance occurs, and we will not consider this extension here.

We now want to write the 1-rsb cavity equation, which is a self-consistent equation for the distribution $P^{(\omega)}$ of local fields h at a *fixed* grand potential ω. $P^{(\omega)}$ is obviously proportional to R, $P^{(\omega)}(h)\propto R(h,\omega)$, and since the distribution of the ω is given by $\int dhR(h,\omega)=C\exp[N\Sigma(\omega)]$, we have the relation

$$R(h,\omega)=Ce^{N\Sigma(\omega)}P^{(\omega)}(h) \tag{39}$$

with C a proportionality constant independent of both h and ω. Next we fix a grand potential density ω_0 and consider only potentials ω close to ω_0, noted $\omega\in\mathcal{V}_{\omega_0}$, such that we can linearize the complexity

$$\Sigma(\omega)\simeq\Sigma(\omega_0)+m\mu(\omega-\omega_0) \tag{40}$$

with

$$m(\omega_0)\equiv\frac{1}{\mu}\frac{d\Sigma}{d\omega}(\omega_0). \tag{41}$$

Given the concavity of the complexity Σ, fixing ω_0 is equivalent to fixing m and thus $\mathcal{V}_{\omega_0}$ can be rewritten as $\mathcal{V}_m$. Plugging relation (39) into Eq. (38), we find that the distribution defined by

$$P^{(m)}(h)\propto\int_{\omega\in\mathcal{V}_m}d\omega P^{(\omega)}(h) \tag{42}$$

satisfies a simple self-consistent equation

$$\begin{aligned}&P^{(m)}(h)\propto\\&\int\prod_{j=1}^{k}dh_jP^{(m)}(h_j)\delta\left(h-\hat{h}(\{h_j\})\right)e^{-m\mu\Delta\hat{\Omega}_{\rm iter}(\{h_j\})}.\end{aligned} \tag{43}$$

Eq. (43) is called the *factorized 1-rsb cavity equation*. We will drop the explicit reference to the parameter m in the ensuing discussion, but it should be kept in mind that the 1-rsb cavity field distribution $P(h)$ is m-dependent.

As we have seen, it is convenient to fix m instead of ω; going from ω to m actually amount to performing a Legendre transformation. The complexity $\Sigma(\omega)$ is recovered by Legendre transforming the function $\Phi(m)$ defined as

$$m\Phi(m)=m\omega-\frac{1}{\mu}\Sigma(\omega) \tag{44}$$

via the relation

$$\frac{1}{\mu}\Sigma(\omega)=m^2\partial_m\Phi(m). \tag{45}$$

Eq. (44) is similar to the definition of the entropy through

$$\mu\omega(\mu)=-\mu\rho-s(\mu) \tag{46}$$

[cf. Eq. (5)]. Indeed $\Phi(m)$ is for the states the analog of the grand potential $\omega(\mu)$ for the configurations, the parameter m sampling the states as the chemical potential μ samples configurations, and the complexity $\Sigma(\omega)$ counting states as the entropy $s(\mu)$ counts configurations [23]. The quantity corresponding to the grand partition function is

$$\begin{aligned}\Xi(m)&=\sum_{\alpha}\exp[-Nm\mu\omega^{(\alpha)}(\mu)]\\&=\int d\omega\exp\left(N[\Sigma(\omega)-m\mu\omega]\right)\\&=\exp[-Nm\mu\Phi(m)].\end{aligned} \tag{47}$$

Following the same analogy, $\Phi(m)$ can be computed similarly to a grand potential. To do so, we first need to generalize to random regular graphs the construction that led

us to the Bethe-Peierls approximation of the grand potential, Eq. (17). Likewise, we want to write

$$\Phi(m) = \Delta\Phi_{\rm site}(m) - \frac{k+1}{2}\Delta\Phi_{\rm edge}(m) \tag{48}$$

with $\Delta\Phi_{\rm site}(m)$ the contribution from a site addition, and $\Delta\Phi_{\rm edge}(m)$ from an edge addition. The way two sites can be added is even simpler than for Bethe lattices here because we do not care about introducing loops: take a random regular graph of size N and connectivity $k+1$, pick $(k+1)$ edges and remove them, leading to $2(k+1)$ amputated sites with k neighbors instead of $(k+1)$. Then add two new sites and connect each one to $(k+1)$ of the amputated sites, leading to a new random regular graph of size $N+2$ and same connectivity $(k+1)$. Thus the contribution to Φ when going from N to $N+2$ sites is equivalent to the contribution from two site additions plus $(k+1)$ edge deletions [i.e., minus $(k+1)$ edge additions], as expressed by Eq. (48).

To see how this is related to the grand potential shifts $\Delta\Omega_{\rm site}$ and $\Delta\Omega_{\rm edge}$, we rewrite Eq. (39) introducing the definition Eq. (41) of the parameter m as

$$R(h,\omega) = e^{m\mu N\left(\omega-\omega^{(0)}\right)}P(h) \tag{49}$$

where $\omega^{(0)} = \omega^{(0)}(m)$ enforces the normalization. The function

$$\rho_0(\Omega) \equiv e^{m\mu\left(\Omega-\Omega^{(0)}\right)} \tag{50}$$

gives the distribution of grand potential $\Omega = N\omega$ on a rooted graph of size N with one site having only k neighbors. Now we take $k+1$ such rooted graphs and determine the distribution $\rho_1(\Omega)$ when one site is added. It is given by

$$\begin{aligned}\rho_1(\Omega) &= \int\prod_{j=1}^{k+1} dh_j d\Omega_j R(h_j,\Omega_j)\delta\left(\Omega - \sum_{j=1}^{k+1}\Omega_j - \Delta\hat{\Omega}_{\rm site}(\{h_j\})\right)\\ &= e^{m\mu\left(\Omega-\sum_{j=1}^{k+1}\Omega_j^{(0)}\right)}\int\prod_{j=1}^{k+1} dh_j P(h_j) e^{-m\mu\Delta\hat{\Omega}_{\rm site}(\{h_j\})}\\ &\equiv e^{m\mu\left(\Omega-\Omega^{(1)}\right)}\end{aligned} \tag{51}$$

with $\Omega^{(1)} = \sum_{j=1}^{k+1}\Omega_j^{(0)} + \Delta\Phi_{\rm site}$, while the mean shift $\Delta\Phi_{\rm site}$ due to a site addition is

$$\Delta\Phi_{\rm site}(m) = -\frac{1}{m\mu}\ln\left[\int\prod_{j=1}^{k+1} dh_j P(h_j) e^{-m\mu\Delta\hat{\Omega}_{\rm site}(\{h_j\})}\right]. \tag{52}$$

We compute similarly the contribution from edge addition,

$$\begin{aligned}\rho_2(\Omega) &= \int\prod_{j=1}^{2} dh_j d\Omega_j R(h_j,\Omega_j)\delta\left(\Omega - \sum_{j=1}^{2}\Omega_j - \Delta\hat{\Omega}_{\rm edge}(h_1,h_2)\right)\\ &= e^{m\mu\left(\Omega-\Omega_1^{(0)}-\Omega_2^{(0)}\right)}\int\prod_{j=1}^{2} dh_j P(h_j) e^{-m\mu\Delta\hat{\Omega}_{\rm edge}(h_1,h_2)}\\ &\equiv e^{m\mu\left(\Omega-\Omega^{(2)}\right)}\end{aligned} \tag{53}$$

with $\Omega^{(2)} = \Omega_1^{(0)} + \Omega_2^{(0)} + \Delta\Phi_{\rm edge}$, while the mean shift $\Delta\Phi_{\rm edge}$ due to an edge addition is

$$\Delta\Phi_{\rm edge}(m) = -\frac{1}{m\mu}\ln\left[\int\prod_{j=1}^{2} dh_j P(h_j) e^{-m\mu\Delta\hat{\Omega}_{\rm edge}(h_1,h_2)}\right]. \tag{54}$$

The replica symmetric description of the liquid phase is recovered by taking $P(h) = \delta(h - h_{\rm liq})$. When many solutions coexist, by varying $m = m(\omega_0)$ at fixed μ, we describe states characterized by different values of ω_0 and the question is which m must be selected to describe the *equilibrium* (glassy) thermodynamics. Following Eq. (47), the grand partition function is

$$\Xi(\mu) = \int d\omega \exp\left(N[\Sigma(\omega) - \mu\omega]\right) \tag{55}$$

and the saddle point method for $N\to\infty$ indicates that the grand potential ω of the dominating states is such that $\mu = \partial_\omega\Sigma(\omega)$. But of course, this saddle equation is relevant only if its solution ω_s lies inside the interval range $]\omega_{\rm min},\omega_{\rm max}[$ where the integral is performed, which corresponds to the range where $\Sigma(\omega)$ is strictly positive. Generically, for $\mu > \mu_s$, it is found that $\omega_s < \omega_{\rm min}$, and we must then take instead $\omega_s = \omega_{\rm min}$. A kind of replica trick intervenes here to balance the complexity contribution thanks to the parameter m, in such a way that ω_s is always given by a saddle equation. So, in the glassy phase $\mu > \mu_s$ where the rsb formalism becomes necessary, we want the equilibrium grand potential to be given by $\omega_s = \omega_{\rm min}(\mu) \equiv \Phi(m_s)$. Since the complexity curve is expected to be continuous at $\omega_{\rm min}$, we can alternatively ask for the condition $\Sigma(\omega_s) = 0$. From Eq. (45), we see that it corresponds to extremizing $\Phi(m)$, i.e.,

$$\partial_m\Phi(m = m_s) \equiv 0 \tag{56}$$

which is precisely the criterion provided by the replica method for selecting the breaking point parameter m.

Note that other values of m also carry physical information. Lower values of m ($m < m_s$) describe metastable states for which $\omega > \omega_s$ (it is the analog of a non-zero temperature giving access to excited configurations); of particular interest is the value ω_d associated to the maximum complexity $\Sigma(\omega_d) \equiv \max_\omega \Sigma(\omega)$ since its describes the most numerous states. We expect that this is the portion

of phase space where the system will get almost trapped at long times after a "quench" from the low density liquid phase.

Higher values of m ($m > m_s$) are usually termed as unphysical, but in fact they describe properties of systems associated with untypical graphs. In particular, it can be shown that $m = 1$ always gives back the liquid solution. In fact, for $m > m_s$, the cavity method leads to a negative complexity, which seems to be in contradiction with its initial definition Eq. (41). The point is that in the cavity method, the graph is not specified and $e^{N\Sigma(\omega)}$ is the number of states with grand potential ω after averaging over different graph realizations. This fact has no consequence whenever the average corresponds to the typical case, which is expected as soon as $\Sigma(\omega) > 0$; indeed some graph realizations may behave very differently from typical realizations, but their contribution to the averaged quantities is negligible. However, an exception is worth mentioning: if the quantity we average is typically strictly zero, but happen to be positive for exponentially rare realizations, it leads to a small but non zero (i.e. non typical) average. We find such a behavior here, where some untypical graphs allow for ω_s lower than the typical value $\omega_s^{(\mathrm{typ})}$, leading to a $\Sigma\left(\omega < \omega_s^{(\mathrm{typ})}\right) < 0$ even if the complexity on a given graph is intrinsically a positive quantity.

An analog phenomenon happens for instance in the random energy model, where averaging over disorder leads to a negative entropy associated with energies lower than the typical ground state, while for a given realization of the disorder the entropy is necessarily positive. Here the role of the quenched disorder is taken by the topological disorder from the various realizations of random regular graphs. From this point of view, a random graph with no frustrating loop is an example of untypical graph which has a crystalline ground state, as opposed to the glassy ground states of typical random regular graphs.

4.5 Observables

To complete our overview of the cavity method, we now show on the example of the particle density how physical observables can be computed; Sect. 4.9 will provide an other example with the computation of susceptibilities. We begin by considering rooted trees where the particle density on the root i is simply given by

$$\langle n_i \rangle_{\text{rooted tree}} = \frac{\Xi_i^{(s)} + \Xi_i^{(u)}}{\Xi_i^{(s)} + \Xi_i^{(u)} + \Xi_i^{(e)}} = 1 - e^{-\mu a_i}. \quad (57)$$

Now for a Cayley tree, we need to take into account $k+1$ neighbors instead of k,

$$\langle n_i \rangle_{\text{Cayley tree}} = 1 - e^{-\mu A_i}. \quad (58)$$

where the total local field A is computed similarly to the cavity field a but substituting k by $k+1$, i.e.,

$$A_i = \hat{A}(a_1, b_1, \ldots, a_{k+1}, b_{k+1}) = \frac{1}{\mu} \ln \left[1 + e^{\mu(1 - \sum_{j=1}^{k+1} a_j)} \left(1 + \sum_{j=1}^{k+1} (e^{\mu b_j} - 1) \right) \right]. \quad (59)$$

The total field B_i would be defined similarly; note that with our notations, we simply have $\hat{A} = -\Delta\hat{\Omega}_{\text{site}}$. On a random graph in the 1-rsb phase, we need to include the reweighting associated with the addition of the site i:

$$\rho(\mu, m) = \frac{\int \prod_{j=1}^{k+1} dh_j P(h_j)(1 - e^{-\mu\hat{A}(\{h_j\})}) e^{-m\mu\Delta\hat{\Omega}_{\text{site}}(\{h_j\})}}{\int \prod_{j=1}^{k+1} dh_j P(h_j) e^{-m\mu\Delta\hat{\Omega}_{\text{site}}(\{h_j\})}} \quad (60)$$

and the equilibrium value is given by $\rho(\mu, m_s)$. The same lines can be followed to compute any other observables.

4.6 Order parameters

Comparing with the replica method [14], the cavity approach focuses on local fields instead of overlaps between states. In lattice glass models, the latter can be defined as

$$q_{\alpha\beta\gamma\ldots} \equiv \frac{1}{N} \sum_{i=1}^{N} \langle n_i \rangle_\alpha \langle n_i \rangle_\beta \langle n_i \rangle_\gamma \ldots \quad (61)$$

with the indices α, β, γ, ... denoting states randomly chosen according to their Boltzmann weights.

Overlaps are particularly useful in infinite connectivity systems where, due to the central limit theorem, the first two moments q_α and $q_{\alpha\beta}$ are sufficient to encode the Gaussian distribution of the cavity fields. In contrast, for finite connectivity systems, an infinite number of overlaps must be kept and working directly with the local field distribution is simpler. However, the two choices of order parameters, local cavity fields or global overlaps, provide complete and equivalent descriptions; in particular overlaps can be easily recovered from the knowledge of the cavity field distribution.

At the replica symmetric level, all indices α, β, γ, ... are equivalent, so we only need to distinguish overlaps according to the number r of states they involve, and we have

$$q_r^{(\mathrm{rs})} \equiv \overline{\langle n_i \rangle^r} = \int dA dB \mathcal{P}_{rs}(A, B) \left(1 - e^{-\mu A}\right)^r \quad (62)$$

with A and B being the total local fields of Sect. 4.5. Note that the replica symmetric approximation in principle already involves a functional order parameter $\mathcal{P}_{rs}$, but in our case where the factorization Ansatz is taken, the liquid distribution is trivial and we merely have $q_r^{(\mathrm{rs})} = (1 - e^{-\mu A_{\mathrm{liq}}})^r$, i.e. the order parameter is a single scalar.

At the one-step level, we need to distinguish whether randomly chosen states are distinct or identical. Thus for overlaps involving two replicas, we can define two parameters, $q_0 \equiv q_{\alpha\beta}$ ($\alpha \neq \beta$) and $q_1 \equiv q_{\alpha\alpha}$, corresponding respectively in spin glasses to the Edwards-Anderson order parameter and the (squared) magnetization. Their computation amounts to calculating densities inside a state, which was the subject of the previous section. Note however that q_0 and q_1 provide only a partial description of the system and the full order parameter has here a functional structure $P(h)$. Any new level of replica symmetry breaking will require considering a more sophisticated order parameter, namely a distribution over the order parameters from the previous level. For instance, the two-step order parameter will be written as a distribution $Q[P]$ over distributions $P(h)$. Describing with this formalism a finite connectivity system with full replica symmetry breaking is therefore rather complicated, and we will limit ourself to at most two levels of replica symmetry breaking in the ensuing discussion.

4.7 Solution via population dynamics

Given the cavity equations (43), we would like to solve them. Since they are essentially functional relations, an analytical treatment is not possible in general. An important exception however is the close-packed limit $\mu \to \infty$; the next section is devoted to this case. Here we consider the more general finite μ situation and use the *population dynamics algorithm* of Ref. [20] to obtain numerical results. The principle of the algorithm is elementary: the distribution $P(h)$ is encoded in a family of M fields $\{h_i\}_{i=1,\dots,M}$ such that

$$P(h) \simeq \frac{1}{M} \sum_{i=1}^{M} \delta(h - h_i), \tag{63}$$

and the cavity field distribution is expressed as the fixed point of the iteration equation

$$P_{g+1}(h) \propto \int \prod_{j=1}^{k} dh_j P_g(h_j) \delta\left(h - \hat{h}(h_1, \dots, h_k)\right) \\ e^{-m\mu\Delta\hat{\Omega}_{\text{iter}}(h_1,\dots,h_k)}. \tag{64}$$

At each step, M new *children* are generated; each is obtained by choosing randomly k *parents* among the population. To take into account the reweighting, we duplicate or eliminate the children according to their weight $e^{-m\mu\Delta\Omega_{\text{iter}}}$ so that we keep a total population of (approximately) M individuals.

However, such a recursion turns out to be unstable and we stabilize it by means of a relaxation parameter $\epsilon \in]0, 1[$. At each step, only a fraction ϵM of the population is regenerated. The reason for this relaxation will be made clearer when we will discuss the stability of the cavity method solution; it will be associated to the instability of the first kind discussed in Sect. 5.2.2.

4.8 Static and dynamical transitions

At low μ, the population dynamics algorithm always converges to the liquid solution, i.e., starting from a population with an arbitrary distribution it converges to a population of identical fields corresponding to the fixed point h_{liq} of $\hat{h}$. When μ is increased, a first non-trivial distribution is found at $\mu = \mu_d$ for $m = 1$. At this point many states exist, but they are only metastable and the statics is still given by the (paramagnetic) liquid state. This ergodicity breaking is called a dynamical phase transition because it is where the equilibrium dynamics should display an ergodic-non ergodic transition (see however the discussion in Sect. 6).

A static phase transition, which is the one relevant at equilibrium, only appears for higher chemical potential, $\mu = \mu_s$, when the configurational entropy vanishes. At this point the grand potential of the 1-rsb solution becomes lower than the one of the liquid and the equilibrium phase transition takes place.

In practice, the dynamical transition point μ_d is found by decreasing μ and looking for the μ where the 1-rsb solution disappears. For the BM, it happens at $\mu_d \simeq 6.4$; more generally for $\ell = 1$ and other k we find $\mu_d < \mu_s$, indicating that the transition is always discontinuous, as could not be directly inferred from the arguments of Sect. 4.2. To obtain μ_s, we calculate explicitly $\partial_m \phi(m, \mu)$ and look for the μ at which $\partial_m \phi(m = 1, \mu) = 0$; for the BM, we obtain $\mu_s \simeq 7$.

4.9 Stability of the one-step solution

To determine whether the equilibrium state is really described by a 1-rsb solution or whether further replica breakings are necessary, one has to study the stability of the 1-rsb solution. In this section we set up the formalism needed to check it. In the following sections we will analyze the stability in the close packing limit ($\mu \to \infty$).

In the 1-rsb phase the Gibbs measure is decomposed in a cluster of different thermodynamic pure states [14]. Thus, there are two different types of instabilities that can show up [14]. First kind: The states can aggregate into different clusters (see Fig. 3). To study this instability one has to compute inter-state susceptibilities:

$$\chi_p^{\text{inter}} = \frac{1}{N} \sum_{i,j} \left(\overline{\langle n_i \rangle \langle n_j \rangle} - \overline{\langle n_i \rangle}\ \overline{\langle n_j \rangle} \right)^p. \tag{65}$$

where the overline denotes an average over the states taken with their Boltzmann weights. Second kind: Each state can fragment in different states (see Fig. 3). To study this instability one has to compute intra-state susceptibilities:

$$\chi_p^{\text{intra}} = \frac{1}{N} \sum_{i,j} \overline{\langle n_i n_j \rangle_c^p}. \tag{66}$$

If any of the intra or inter-state susceptibilities diverge then the 1-rsb glass phase is unstable (toward a 2-rsb glass

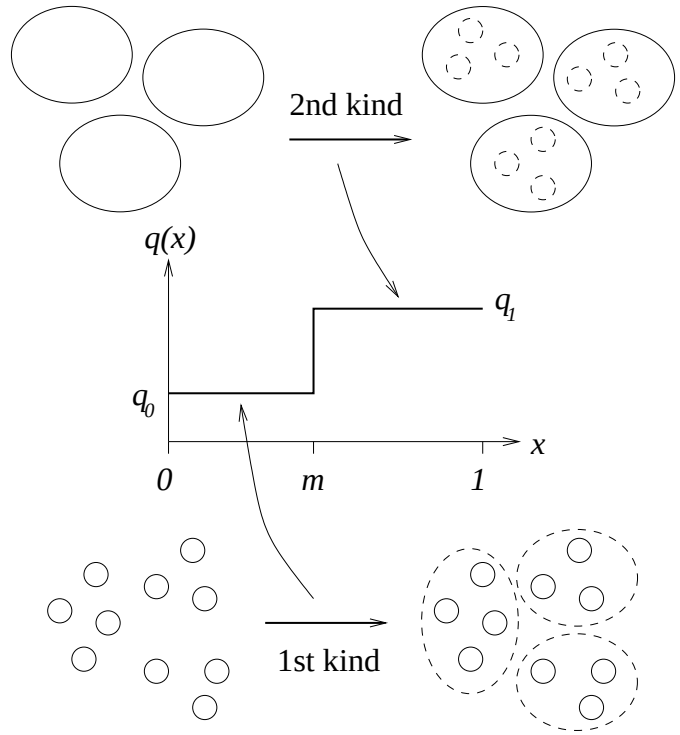

Fig. 3. Pictorial view of the two possible instabilities of the 1-rsb Ansatz. At the bottom, the states stay states but clusterize (first kind). At the top, the states become cluster of new states (second kind). If we were on a totally connected graph where an overlap function $q(x)$ can be defined, its 1-rsb shape would be affected on different parts depending on which instability is relevant; indeed its left part ($x < m$) corresponds to the inter-state overlap q_0 and its right part ($x > m$) to the intra-state overlap q_1.

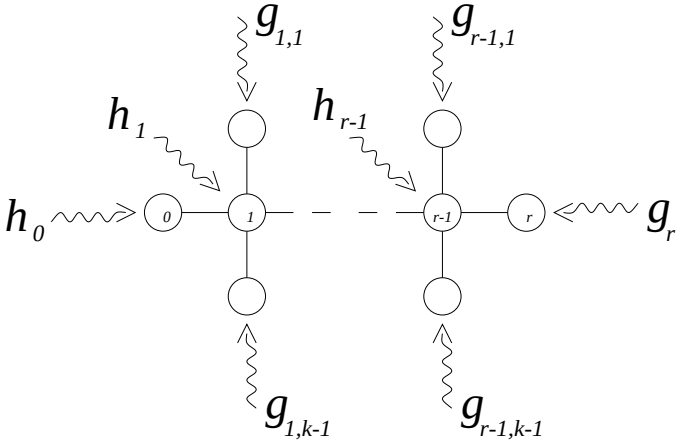

Fig. 4. Cavity diagram for computing a two-site correlation function $\langle n_0 n_r\rangle_c$. As all we know is $P(h)$, the distribution of the local field on the root of a rooted tree, we build a chain of sites $l = 0, \dots, r$ out of rooted trees with fields $h_0, g_{1,j}, \dots, g_{r-1,j}, g_r$. We proceed recursively: we first add site $l = 1$, obtain a new rooted tree with root 1 and local field $h_1 = \hat{h}(h_0, g_{1,1}, \dots, g_{1,k-1})$ so the length of the chain to compute is reduced from $r+1$ to r. Then we proceed further by adding site 2, etc (see also Fig. 5).

phase). However, as for the liquid, the linear susceptibilities χ_1 are related to instabilities incompatible with the underlying random graph structure and, hence, they are irrelevant for our purposes. In the following we will focus on the $p = 2$ case which is the only relevant one since all the susceptibilities with $p > 2$ are clearly bounded in modulus by the $p = 2$ one.

Because of the homogeneity of the simple random graphs that we are focusing on, the stability analysis is simplified and in particular:

$$\begin{aligned}\chi_2^{\text{inter}} &= \sum_{r=1}^{\infty}(k+1)k^{r-1}\left(\overline{\langle n_0\rangle\langle n_r\rangle} - \rho^2\right)^2,\\ \chi_2^{\text{intra}} &= \sum_{r=1}^{\infty}(k+1)k^{r-1}\overline{\langle n_0 n_r\rangle_c^2}\end{aligned} \tag{67}$$

where n_0 and n_r are at distance r (we omitted the unimportant $r = 0$ term).

We expect, as it can be proved (see below), that the correlation functions decay exponentially at large distance

$$\overline{\langle n_0 n_r\rangle_c^2} \sim \exp(-r/\xi_2), \tag{68}$$

and

$$\left(\overline{\langle n_0\rangle\langle n_r\rangle} - \rho^2\right)^2 \sim \exp(-r/\zeta_2). \tag{69}$$

Due to the tree-like structure of the lattice, the resulting stability conditions are different from the condition $\xi < \infty$ used for finite dimension lattices and reads

$$\xi_2 < \frac{1}{\ln k} \qquad , \qquad \zeta_2 < \frac{1}{\ln k}. \tag{70}$$

In the following we show how the correlation length ξ_p can be computed. A very similar procedure can be carried out for ζ_2. In Appendix B we shall show explicitly how this can be done in the close-packing limit ($\mu = \infty$).

In order to obtain ξ_p we need to compute the correlation functions $\overline{\langle n_0 n_r\rangle_c^p}$. We write the generalization of Eq. (28) as

$$\langle n_0 n_r\rangle_{\alpha,c} = \left(\frac{\partial\langle n_r\rangle}{\partial h_{r-1}}\right)^t \left(\prod_{l=1}^{r-1}\partial_1\hat{h}(h_{l-1}; g_{l,j})\right)\frac{\partial h_0}{\partial h_0^{(c)}} \tag{71}$$

where the fields are $(d-1)$-dimensional vectors ($d = 3$ for our models), so that the product involves in fact $(d-1)\times(d-1)$ dimensional Jacobian matrices $\partial_1\hat{h}$ (the notation $\partial_1\hat{h}$ indicates that the derivative is taken with respect to the first field, here h_{l-1}, and $()^t$ means transposed). Note that $\hat{h}(h_{l-1}; g_{l,j})$ is used as a short-hand notation for $\hat{h}(h_{l-1}, g_{l,1}, \dots, g_{l,k-1})$ (see Fig. 4). Next we need to take into account the reweighting introduced by the addition of the sites $l = 1, \dots, r-1$. With a transfer-matrix

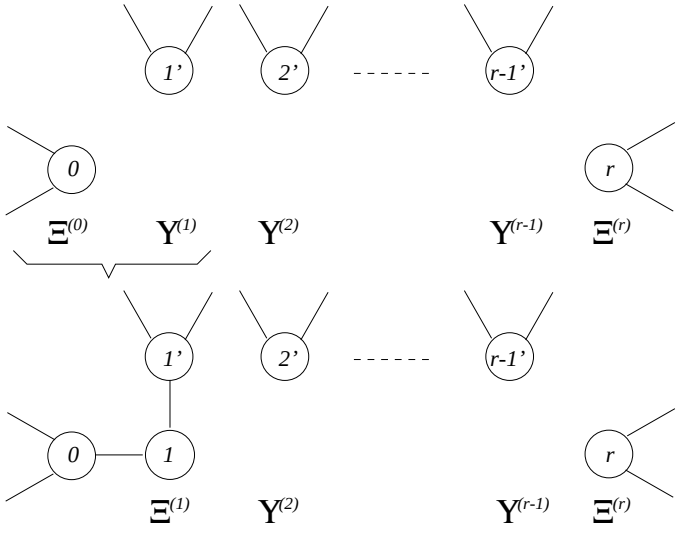

Fig. 5. Partition functions involved in the reweighting for the computation at the 1-rsb level of the two-site correlation $\overline{\langle n_o n_r \rangle^p_{\alpha,c}}$, illustrated here with $k = 2$. We start with the partition functions $\Xi^{(0)}, \Upsilon^{(1)}, \ldots, \Upsilon^{(r-1)}, \Xi^{(r)}$ where $\Upsilon^{(l)}$ is in general the product of the partition functions of $k-1$ rooted trees (top of the figure); for $k = 2$ as illustrated, it reduce to one rooted tree with root site noted l'. Next we merge the k rooted trees corresponding to $\Xi^{(0)}$ and $\Upsilon^{(1)}$ into a site 1 and call the partition function of the resulting rooted tree $\Xi^{(1)}$ (bottom). Recursively, we define similarly the other $\Xi^{(l)}$ for $2 \leq l \leq r-1$.

approach in mind, we write it as

$$e^{-m\mu\Delta\Omega} = \frac{\Xi}{\Xi^{(0)}\left(\prod_{l=1}^{r-1}\Upsilon^{(l)}\right)\Xi^{(r)}} = \prod_{l=1}^{r-1}\left(\frac{\Xi^{(l)}}{\Xi^{(l-1)}\Upsilon^{(l)}}\right)\frac{\Xi}{\Xi^{(r-1)}\Xi^{(r)}} \tag{72}$$

where the notation refers to Fig. 5: $\Upsilon^{(l)}$ denotes the product of the $k-1$ partition functions associated with the rooted trees with cavity fields $g_{l,j}$ $(1 \leq j \leq k-1)$ and $\Xi^{(l)}$ $(1 \leq l \leq k-1)$ the partition function of the rooted tree obtained by connecting a new site l to the k rooted trees corresponding to $\Upsilon^{(l)}$ and $\Xi^{(l-1)}$.

We can write for one site addition

$$\frac{\Xi^{(l)}}{\Xi^{(l-1)}\Upsilon^{(l)}} = \exp[-m\mu\Delta\hat{\Omega}_{\rm iter}(h_{l-1}; g_{l,j})], \tag{73}$$

and for the last edge addition

$$\frac{\Xi}{\Xi^{(r-1)}\Xi^{(r)}} = \exp[-m\mu\Delta\hat{\Omega}_{\rm edge}(h_{r-1}, g_r)]. \tag{74}$$

The 1-rsb formula for $\overline{\langle n_0 n_r \rangle^p_c}$ is therefore

$$\mathcal{Z}^{-1}\int dh_0 P(h_0)\left[\prod_{l=1}^{r-1}\left(\prod_{j_l=1}^{k-1} dg_{l,j_l}P(g_{l,j_l})\right)\right]dg_r P(g_r) \left[\left(\frac{\partial\langle n_r\rangle}{\partial h_{r-1}}\right)^t\left(\prod_{l=1}^{r-1}\partial_1\hat{h}(h_{l-1}; g_{l,j})\right)\frac{\partial h_0}{\partial h_0^{(c)}}\right]^p \left(\prod_{l=1}^{r-1} e^{-m\mu\Delta\hat{\Omega}_{\rm iter}(h_{l-1};g_{l,j})}\right) e^{-m\mu\Delta\hat{\Omega}_{\rm edge}(h_{r-1},g_r)} \tag{75}$$

where the normalization $\mathcal{Z}$ is given by

$$\mathcal{Z} = \int dh_0 P(h_0)\left[\prod_{l=1}^{r-1}\left(\prod_{j_l=1}^{k-1} dg_{l,j_l}P(g_{l,j_l})\right)\right]dg_r P(g_r) \left(\prod_{l=1}^{r-1} e^{-m\mu\Delta\hat{\Omega}_{\rm iter}(h_{l-1};g_{l,j})}\right) e^{-m\mu\Delta\hat{\Omega}_{\rm edge}(h_{r-1},g_r)}. \tag{76}$$

To be complete, we also need to insert in the previous formulae the following identity defining the intermediate fields h_l,

$$1 = \int\prod_{l=1}^{r-1} dh_l \delta\left(h_l - \hat{h}(h_{l-1}; g_{l,j})\right). \tag{77}$$

To determine the behavior of the correlation functions between sites at distance r, we introduce two transfer matrices, corresponding respectively to the numerator and denominator of Eq. (75),

$$T_n(h_{l-1}, h_l) = \int\prod_{j_l=1}^{k-1} dg_{l,j_l}P(g_{l,j_l})\partial_1\hat{h}(h_{l-1}, g_{l,j_l}) \delta\left(h_l - \hat{h}(h_{l-1}; g_{l,j_l})\right) e^{-m\mu\Delta\hat{\Omega}_{\rm iter}(h_{l-1};g_{l,j_l})},$$
$$T_d(h_{l-1}, h_l) = \int\prod_{j_l=1}^{k-1} dg_{l,j_l}P(g_{l,j_l}) e^{-m\mu\Delta\hat{\Omega}_{\rm iter}(h_{l-1};g_{l,j_l})} \delta\left(h_l - \hat{h}(h_{l-1}; g_{l,j_l})\right). \tag{78}$$

Finally, calling respectively $\lambda_n^{(p)}, \lambda_d$ the largest eigenvalues of the matrices $(T_n)^p$ and T_d we obtain that for large r

$$\overline{\langle n_0 n_r \rangle^p_c} \sim \exp(-r/\xi_p) \tag{79}$$

with

$$\xi_p = -\frac{1}{\ln(|\lambda_n^{(p)}/\lambda_d|)}. \tag{80}$$

Notice that all this discussion of stability of the 1-rsb solution is not just academic. Indeed simulations performed on the BM with the distribution P of the fields $g_{l,j}$ generated by population dynamics show that, at a fixed

chemical potential $\mu > \mu_d$, the correlation length $\xi_2(m)$ increases when m is decreased from $m = 1$ to 0. In addition, the critical length $1/\ln 2$ is reached at some finite value of m, $m_c < m_s$, indicating that the description of metastable states corresponding to $m < m_c$ requires to break the replica symmetry beyond one step.

The limits of the 1-rsb approach will be discussed in much more details in the following section devoted to the $\mu = \infty$ limit where it is shown that the $[((d-1)\infty) \times ((d-1)\infty)]$ transfer "matrices" (the ∞ stands for the continuum range of the fields h_l so the matrices are actually operators) reduce to finite $[(d-1)d \times (d-1)d]$ matrices whose eigenvalues can be computed without resorting to the population dynamics.

5 Close-packing limit

The zero temperature limit of the cavity method, which corresponds in lattice glasses to the $\mu = \infty$ limit, has received particular attention [24], both because of the simplifications it allows and because of its applications to optimization problems. For lattice glasses, the corresponding optimization problem, called the *close-packing problem*, consists in finding, for given lattice and packing constraint, the largest achievable particle density. We will obtain the solution of this problem as a result of our study.

5.1 One-step rsb Ansatz

We first consider the close-packing problem as a limiting case of the previous considerations; thus for $\mu \to \infty$, the single rs equations (3.1) and (12) simplify to

$$a_0 = \max\left(0, 1 - \sum_{j=1}^{k} a_j + \max_{1\le j\le k} b_j\right), \tag{81}$$

$$b_0 = \max\left(0, 1 - \sum_{j=1}^{k} a_j\right). \tag{82}$$

The advantage of this limit is that we can resort to the exact Ansatz

$$\begin{aligned} P(a,b) =& p_e\delta(a)\delta(b) + p_u\delta(a-1)\delta(b-1) \\ &+ (1-p_e-p_u)\delta(a-1)\delta(b). \end{aligned} \tag{83}$$

Note that the simple form obtained here results from our appropriate choice of the local fields. Other choices may lead to a similar Ansatz but with more than three spikes. This minimal number of three is related to the three "degrees of freedom" of our model, as appeared clearly when we needed three conditional partition functions. (In general the number of spikes will be the minimum necessary number of local fields plus one).

This Ansatz is certainly the only one with integer fields, and at this stage it is not obvious why we should not consider other solutions of Eq. (81-82) with non integer fields. However the reason to take integer fields appears clearly when working directly at $\mu = \infty$. Indeed, the local fields have then a simple interpretation in term of the number of particles and must therefore be integers. To see why, go back to the recursion on rooted trees and note $N_i^{(e)}$, $N_i^{(u)}$ and $N_i^{(s)}$ the numbers of particles of a (finite) rooted tree when its root node i is empty (e), occupied but the constraint unsaturated (u) and finally occupied and the constraint saturated (s), i.e., the root site has ℓ neighboring particles. Considering as before the $\ell = 1$ case, we have

$$\begin{aligned} N_0^{(e)} &= \sum_{j=1}^{k} \left(N_j^{(e)} + N_j^{(u)} + N_j^{(s)}\right), \\ N_0^{(u)} &= 1 + \sum_{j=1}^{k} N_j^{(e)}, \\ N_0^{(s)} &= 1 + \max_{1\le j\le k} N_j^{(u)} \sum_{p\neq j_{\max}} N_p^{(e)} \end{aligned} \tag{84}$$

where $N_{j_{\max}}^{(u)} \equiv \max_{1\le j\le k} N_j^{(u)}$. Obviously, this is nothing but the corresponding $\mu \to \infty$ limit of the Eq. (6-8) with $\Xi^{(a)} \sim \exp\left(\mu N^{(a)}\right)$, $a = e, u, s$. The corresponding local fields are

$$\begin{aligned} a_i &= \max\left(N_i^{(e)}, N_i^{(u)}, N_i^{(s)}\right) - N_i^{(e)}, \\ b_i &= \max\left(N_i^{(e)}, N_i^{(u)}\right) - N_i^{(e)}. \end{aligned} \tag{85}$$

It is now clear that we can only have $a_i, b_i \in \{0, 1\}$ with in addition $b_i \le a_i$. Moreover, one has a simple interpretation of the three spikes.

Plugging the Ansatz in the general 1-rsb cavity equation Eq. (43) and taking $y \equiv \lim_{\mu\to\infty} \mu m$ as breaking parameter we get

$$p_e = Z^{-1}\left(1 - p_e^k - k p_e^{k-1} p_u\right), \tag{86}$$

$$p_u = Z^{-1} p_e^k e^y, \tag{87}$$

$$Z = 1 + (e^y - 1)(p_e^k + k p_e^{k-1} p_u). \tag{88}$$

These equations are in fact very simple and can be found following the principle that for $\mu = \infty$ a particle must be present whenever it is allowed. So in terms of the state of the root, the merging of rooted graphs gives:

$$\begin{aligned} &\underbrace{e + \cdots + e}_{k} \to u \\ &u + \underbrace{e + \cdots + e}_{k-1} \to s \\ &\text{all other combinations} \to e \end{aligned} \tag{89}$$

which simply means that k empty sites lead to an occupied unsatured site, $k-1$ empty sites with one occupied unsatured leads to an occupied saturated sites and all other cases yield an empty site. Now call p_e, p_u and p_s the probabilities to be respectively in states e, u and s; the three

rules translate into three self-consistent equations

$$\begin{aligned} p_u &\propto p_e^k e^y \\ p_s &\propto k p_u p_e^{k-1} e^y \\ p_e &\propto 1 - p_e^k - k p_u p_e^{k-1} \end{aligned} \tag{90}$$

which are exactly the 1-rsb equations (86-87) for $\mu = \infty$ when the normalization $p_e + p_u + p_s = 1$ is taken into account. The reweighting factor e^y is introduced each time the recursion adds a particle since in this case we have a "density shift" $\Delta N = 1$.

As before, the equilibrium value of the grand potential is given by the maximum at $y = y_s$ of $\phi(y)$ with here

$$\begin{aligned} -y\phi(y) = &\ln\left[1 + (e^y - 1)(p_e^{k+1} + (k+1)p_e^k p_u)\right] \\ &- \frac{k+1}{2}\ln\left[1 + (e^{-y} - 1)((1-p_e)^2 - p_u^2)\right]. \end{aligned} \tag{91}$$

The configurational entropy $\Sigma(\rho)$ as a function of the density ρ is defined by the parametrized curve

$$\Sigma(y) = y^2 \partial_y \phi(y), \tag{92}$$
$$\rho(y) = -\partial_y [y\phi(y)]. \tag{93}$$

Note that since $\partial_y \phi(y_s) = 0$, we have for the solution of the close-packing problem

$$\rho_\infty = \rho(y_s) = -\phi(y_s). \tag{94}$$

The complexity Σ has a maximum at $\rho_d = \rho(y_d)$ where y_d is given by $\partial_y^2 [y\phi(y)] = 0$. The curve displays a non concave part for $y < y_d$ which may not have any physical interpretation; anyway, we will see that this unexpected part belongs to a region of the parameter y where the results of a 1-rsb calculation are unreliable. In Fig. 6, we present the complexity curve for the BM. The close-packing densities of various models are presented in Fig. 7.

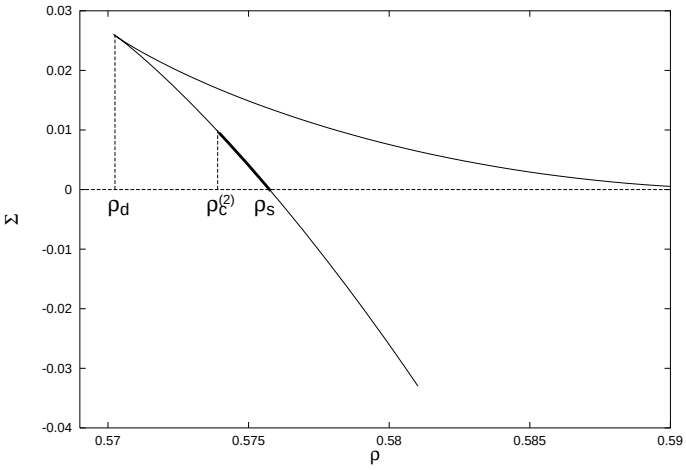

Fig. 6. Complexity curve $\Sigma(\rho)$ obtained from the 1-rsb Ansatz for the BM in the close-packing limit $\mu = \infty$; its slope corresponds to $-y$. Four parts of the curve can be distinguished. First, a negative part ($y > y_s$) due to the contribution of untypical graphs with few frustrating loops. For $\rho_c^{(2)} < \rho < \rho_s$, i.e., $y_c^{(2)} < y < y_s$ (bold part), the 1-rsb Ansatz is stable and ρ_s where $\Sigma = 0$ gives the close-packing density. The complexity curve for $\rho < \rho_s$ corresponds to metastable states; it is no longer correctly described by the 1-rsb Ansatz for $\rho < \rho_c^{(2)}$ ($y < y_c^{(2)}$). Finally, we obtain for the fourth part an unphysical non concave branch.

ℓ	k	ρ_s	ρ_d	$\rho_c^{(2)}$
1	2	0.575742	0.5703	0.5739
1	3	0.517288	0.5097	0.5159
1	4	0.473384	0.4646	0.4728
1	5	*0.438382*	0.4288	frsb
2	2	0.735050	0.7302	0.7337
2	3	0.636187	0.6256	0.6223
2	4	0.573723	0.5606	0.5701
2	5	0.527301	0.5129	0.5247
3	3	0.776695	0.7748	0.7682
3	4	0.680316	0.6660	0.6755
3	5	0.617160	0.6001	0.6123
4	4	0.805338	0.7945	0.8033
4	5	0.713982	0.6972	0.7088
5	5	0.826487	0.8140	0.8245

Fig. 7. Close-packing densities $\rho_\infty = \rho_s$ for random regular graphs of connectivity $k+1$ ($k = 5$ approximates the three dimensional cubic space) where each particle can have no more than ℓ neighboring particles. We indicate the dynamical density ρ_d where the complexity is maximum; any local algorithm trying to determinate ρ_s will stay in the region where $\rho < \rho_d$. We emphasize however that this value is only a 1-rsb approximation (possibly an upper bound) which we have shown to be wrong due to the instability of second kind toward further rsb; $\rho_c^{(2)}$ gives the value of the density where this instability occurs and thus provides a lower bound for the correct ρ_d. Note that for $\ell = 1$, $k = 5$ even the equilibrium density ρ_s is not correctly described by an 1-rsb Ansatz.

5.2 Stability of the 1-rsb Ansatz

Having derived the $\phi(y)$ function analytically, it is interesting to compare it with the output of the population dynamics algorithm. As a first consistency check, it is observed that when the population is started on the integer spikes, both approaches lead exactly to the same result. However, considering the stability of the integer Ansatz under population dynamics provides additional features. For large y, $y \geq y_c^{(2)}$, it is found that even when starting with arbitrary fields, the dynamics converges to the expected distribution on the integers; however for $y \leq y_c^{(2)}$, this Ansatz is found to be unstable and the population dynamics converges to a new continuous distribution, corresponding to a greater $\phi(y)$, as displayed in Fig. 8. This behavior looks puzzling at first sight since on the one hand we know that the fields must be integer, and on the other hand the cavity method is known to lead to a lower bound

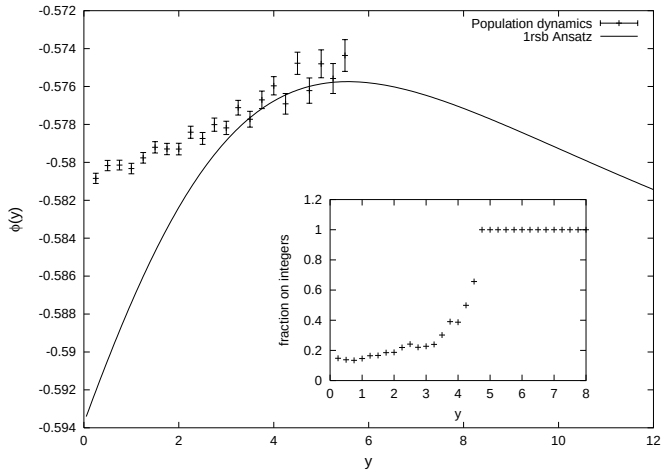

Fig. 8. $\phi(y)$ for the BM ($\ell = 1$, $k = 2$) in the close-packing limit $\mu = \infty$. The bold line is the result of the 1-rsb Ansatz. Its maximum at $y_s \simeq 5.56$ gives the close-packing density $\rho_s = -\phi(y_s) \simeq 0.5757$. The points with error bars were obtained with the population dynamics algorithm after 1000 iterations of a population of 10000 fields. We clearly obtain two different results for low y. Note that when y increase, error bars increases, due to larger and larger reweighting factors, making $\phi(y)$ an average dominated by a few large terms only; this is why we do not display population dynamics results for large y where anyway we know that the 1-rsb Ansatz should be recovered. A numerical check of this point is provided by studying directly the distribution of the fields. In the inset, we show how the fraction of the population within $\delta = 0.01$ of one of the three spikes predicted by the 1-rsb Ansatz evolves with y. We thus verify that when $y > y_c^{(2)} \simeq 5.06$, the population is entirely on the peaks, even though it was started with an arbitrary distribution.

of the grand potential [25], so given two different solutions for $\phi(y)$, we must choose the larger. The explanation for this contradiction must be that the approximation we used, namely the 1-rsb formalism, is not valid. Therefore, we expect that further replica symmetry breaking occurs for the metastable states with $y \leq y_c^{(2)}$, a situation that has been argued to be a generic feature of discontinuous spin glasses [26].

We now present how the exact value $y_c^{(2)}$ can be computed. As when dealing with the liquid instability, two approaches are possible. We can either resort to the stability of the local fields distribution under the cavity recursion, which requires to place oneself in a two-step cavity formalism, or we can stay at the one-step level and consider diverging response functions. The $\mu \to \infty$ limit of the formalism described in Sect. 4.9 is a bit tricky because correlations are trivial in the $\mu = \infty$ limit: $\overline{\langle n_0 n_r \rangle_c} = 0$, due to a total freezing within each state. The stability analysis based on response functions is still possible, but must not rely on susceptibilities; this procedure is presented in Appendix B. Here, we will adopt an equivalent approach based on the 2rsb formalism, following [26].

5.2.1 Two-step replica symmetry breaking cavity method

To emphasize the generality of the discussion, let us consider a generic 1-rsb solution at infinite μ given by a field distribution

$$P^*(h) = \sum_{a=1}^{d} p_a \delta(h - h_a) \equiv \sum_{a=1}^{d} p_a \delta_a(h) \qquad (95)$$

peaked on d cavity fields, each having $(d-1)$ components that are integer valued [$d = 3$ for all (k, ℓ) lattice glasses]. The p_a satisfy a relation analogous to Eq. (86) and (87),

$$p_a = \frac{1}{Z} \sum_{(b_1,\dots,b_k)\to a} p_{b_1} \dots p_{b_k} \exp[-y \Delta E_{b_1,\dots,b_k}]. \qquad (96)$$

Note that the fields are such that there is no degeneracy, i.e., k parents in configurations $(b_1, \dots, b_k)$ lead to a child whose configuration can only be a.

At the two-step level, not only the configurations are grouped into different states, requiring to consider a distribution $P(h)$ over these states, but the states are themselves organized into larger clusters, that is groups of states sharing some common properties. We therefore need to consider a probability distribution $Q[P]$ over the probability distributions $P(h)$. It has the following meaning: on a given site, the distribution $P_c(h)$ of the cavity field inside a cluster c must be taken from the distribution $Q[P]$.

The 2-rsb cavity equations are obtained by generalizing the 1-rsb distribution $\mathcal{N}_N(\omega) \sim e^{Ny(\omega-\omega_0)}$ of the number of states with fixed ω to

$$\mathcal{N}_N(\omega) \sim \int d\omega_1 d\omega_2 \delta(\omega - \omega_1 - \omega_2) e^{N y_1 (\omega_1 - \omega_0)} e^{N y_2 (\omega_2 - \omega_1)}. \qquad (97)$$

Here ω is decomposed into $\omega_1 + \omega_2$ with ω_1 the grand potential of a cluster with respect to a reference ω_0, and ω_2 the grand potential of a state inside the cluster with respect to that of the cluster ω_1. The hierarchical rsb scheme is here reflected by the similarity between the distributions of ω_1 and ω_2, $\mathcal{N}_N^{(1)}(\omega_1|\omega_0) \sim \exp[N y_1 (\omega_1 - \omega_0)]$ and $\mathcal{N}_N^{(2)}(\omega_2|\omega_1) \sim \exp[N y_2 (\omega_2 - \omega_1)]$. Starting from the distribution given by Eq. (97) and following the lines of the derivation of the 1-rsb cavity equation described in Sect. 4.4, we obtain the 2-rsb cavity equation

$$Q[P] = \frac{1}{Z} \int \prod_{j=1}^{k} \mathcal{D}P_j Q[P_j] \hat{z}[\{P_j\}]^{y_1/y_2} \delta[P - \hat{P}[\{P_j\}]] \qquad (98)$$

where

$$\hat{P}[\{P_j\}] = \frac{1}{\hat{z}[\{P_j\}]} \int \prod_{j=1}^{k} dh_j P_j(h_j) \delta(. - \hat{h}(\{h_j\})) \exp(-y_2 \Delta \hat{E}(\{h_j\})) \qquad (99)$$

and

$$\hat{z}[\{P_j\}] = \int \prod_{j=1}^{k} dh_j P_j(h_j) \exp(-y_2 \Delta \hat{E}(\{h_j\})). \qquad (100)$$

The Parisi parameters y_1 and y_2 have to be taken such that $y_1 \leq y_2$. Note that in particular, for $y_1 = 0$ and $y_2 = y$ (y denotes the 1-rsb parameter), the formalism describes a non-factorized 1-rsb solution.

It is essential to understand how the 1-rsb Ansatz must be written in this 2-rsb formalism. Two scenarios are indeed possible. Either the 1-rsb states coincide with the 2-rsb states and there is just one trivial 2-rsb cluster, or the 1-rsb states coincide with the 2-rsb clusters and 2-rsb states reduce to single configurations. Within the first scenario, the one-step corresponds to $Q = \delta[P - P^*]$ where $P^* = \sum_a p_a \delta_a$ is the one-step probability distribution of Eq. (95) while within the second scenario, the one-step corresponds to $Q[P] = \sum_a p_a \delta[P - \delta_a]$.

Depending on which case we consider, we can have two possible kinds of instabilities, as first noted by Montanari and Ricci-Tersenghi [26]. As in Sect. 4.9, in the first case, the states gather into different clusters, while in the second case new states appear within the old states which therefore become clusters. A pictorial view is given in Fig. 3.

5.2.2 Instability of the first kind: aggregation of states

The instability of first kind can be studied by considering an Ansatz of the form

$$Q[P] = f[P - P^*] \tag{101}$$

where f is a functional with support around the null function. The instability is given by the eigenvalue of largest modulus $\Lambda_1(y)$ of the Jacobian matrix associated with Eq. (96). Here again, as we deal with random graphs we ignore the modulation instability $k|\Lambda_1| > 1$ and focus on the glass instability $\sqrt{k}|\Lambda_1| > 1$. Different cases are observed as we vary the parameters ℓ and k in our lattice glass models. In some cases the instability is absent and appears only asymptotically, i.e., we have $\sqrt{k}|\Lambda_1(y)| < 1$ for all y but $\sqrt{k}|\Lambda_1(y)| \to 1$ as $y \to \infty$; this happens on low connectivity graphs, e.g. for $k = 2, 3$ when $\ell = 1$. At higher connectivities, we can define a critical $y_c^{(1)}$ such that $\sqrt{k}|\Lambda_1(y)| > 1$ for $y > y_c^{(1)}$. Then we have to determine the relative position of $y_c^{(1)}$ with respect to y_s giving the maximum of $\phi(y)$. Fig. 9 shows how y_s and $y_c^{(1)}$ evolve with the connectivity $k + 1$ for the case $\ell = 1$. When $y_s < y_c^{(1)}$, as it is found for $k = 4, 5$ for $\ell = 1$, the positive part of the complexity curve is unaffected and we can rely on our 1-rsb description for typical graphs. However, if $y_s > y_c^{(1)}$, as we find when $6 \leq k \leq 25$, the 1-rsb treatment is not stable, and one should develop a higher order rsb formalism.

5.2.3 Instability of the second kind: fragmentation of states

To study the instability of second kind, we consider an Ansatz of the form

$$Q[P] = \sum_a p_a f_a[P - \delta_a] \tag{102}$$

where the f_a have support around the null function. Since P is necessarily a combination of the δ_e, the argument of f_a can be written as $\delta P \equiv P - \delta_a = \sum_{e \neq a} \epsilon_e (\delta_e - \delta_a)$ and we evaluate the widening of the f_a by computing $\langle \delta P \rangle_a \equiv \int \mathcal{D}\delta P f_a(\delta P)$ to obtain the following relations:

$$\begin{aligned}\langle \epsilon_e \rangle_a =& \frac{k}{Z p_a} \sum_{(b_1 \dots b_k) \to a} p_{b_1} \dots p_{b_k} e^{(y_2 - y_1) \Delta E_{b_1, \dots, b_k}} \\ & \sum_{c \neq b_1, (c, b_2, \dots, b_k) \to e} e^{-y_2 \Delta E_{c, b_2, \dots, b_k}} \langle \epsilon_c \rangle_{b_1}.\end{aligned} \tag{103}$$

Since we consider a local instability of the 1-rsb solution we take $y_1 = y_2 = y$. Noting $\lambda_{a \to e} \equiv \langle \epsilon_e \rangle_a$ it reads

$$\begin{aligned}p_a \lambda_{a \to e} =& \frac{1}{Z} \sum_{(b_1, \dots, b_k) \to a} p_{b_1} \dots p_{b_k} \\ & \sum_{j, c \neq b_j, (b_1, \dots, c, \dots, b_k) \to e} e^{-y \Delta E_{b_1, \dots, c, \dots, b_k}} \lambda_{b_j \to c}.\end{aligned} \tag{104}$$

This notation emphasizes the relation with the point of view based on response functions developed in Appendix B: $p(e|a) \equiv p_a \lambda_{a \to e}$ is the probability to replace a with e by changing only one parent. Indeed, for $\mu \to \infty$, adding a small perturbating field is equivalent to changing a configuration a. The equation tells us how such a change propagates from a site to its neighbor.

As expected from Sect. 4.9, the instability is described by a $[d(d-1)] \times [d(d-1)]$ transfer matrix $T_{ad,bc}$, $\langle \epsilon_e \rangle_a = k \sum_{b \neq c} T_{ae,bc} \langle \epsilon_c \rangle_b$. If Λ_2 is the eigenvalue of T of largest modulus, the one-step solution is stable provided $k\Lambda_2 \leq 1$ (Λ_2 is positive, due to Perron-Frobenius theorem); here we need not square the eigenvalues since the first moments $\langle \epsilon_e \rangle_a$ does not vanish due to the positivity of the $\lambda_{a \to e}$ (since Λ_2 is positive the instability detected by $k\Lambda_2 = 1$ is compatible with the underlying random lattice). Note that the same principles are straightforwardly extendable to cases with fluctuating connectivity and/or quenched disorder; we would have to average over the different possible transfer matrices.

We present in Appendix C a simple method to obtain the transfer matrix T and focus here on the results. Generically, it is found that $k\Lambda_2 < 1$ for large enough y, $y > y_c^{(2)}$. For instance for the BM, we obtain $y_c^{(2)} \simeq 5.061$. This instability is precisely the one detected by the population dynamics algorithm. To underline this point, we determine the fraction of the population within $\delta = .01$ of one the $d = 3$ expected delta peaks after 1000 iterations. At $y = 5.06$, this fraction is found to represent 99.2 % of the total population composed of 50000 individuals, while for $y = 5.07$ (and all larger values) it is found to be 100 % as shown in the inset of Fig. 8. We can thus conclude that the onset of non integer fields in the population dynamics is a clear sign that the replica symmetry must be broken beyond one step.

When comparing $y_c^{(2)}$ with y_s, the value of y for which $\phi(y)$ taken with the 1-rsb Ansatz is maximum, we find

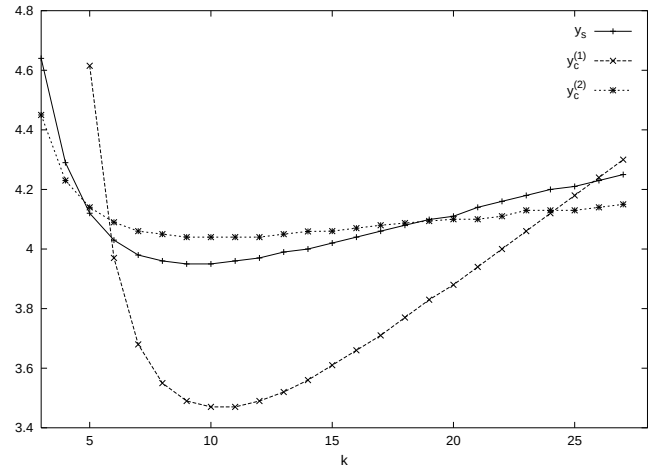

Fig. 9. For $\ell = 1$ and various k, values of the parameters y_s, $y_c^{(1)}$ and $y_c^{(2)}$ giving respectively the equilibrium thermodynamics, the instability of the first kind (for $y > y_c^{(1)}$) and of the second kind (for $y < y_c^{(2)}$). Only if $y_c^{(2)} < y_s < y_c^{(1)}$ is the close-packing limit correctly described by the 1-rsb Ansatz. That is the case for $k \leq 4$ and $k \geq 26$. The lines are only guides for the eyes (we omitted $y_c^{(1)} \simeq 7.0$ for $k = 4$).

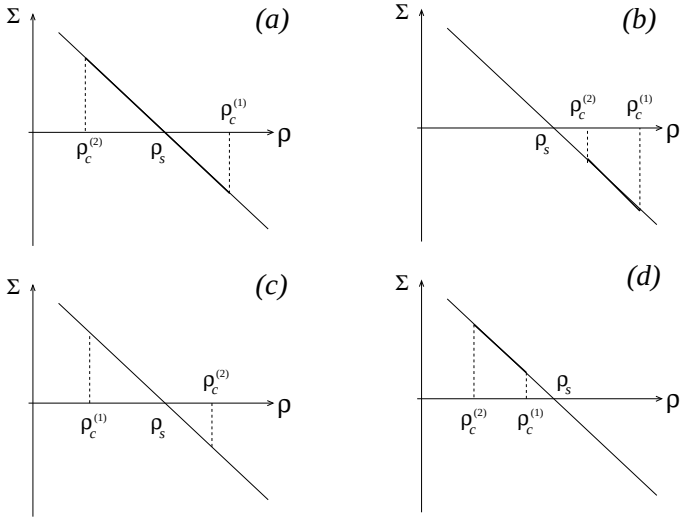

Fig. 10. Part of the complexity curve (bold line) correctly described by the 1-rsb Ansatz. For $\ell = 1$, the case (a) is realized for $k = 2, 3, 4$; the models with $k = 2$ (BM) and $k = 3$ have in fact no instability of the first kind, i.e., the whole $\rho > \rho_c^{(2)}$ range is stable. Case (b), realized for $k = 5$, corresponds to a frsb close-packing, as well as case (c) and (d). In case (c) no part of the 1-rsb complexity curve is correct; this happens for $6 \leq k \leq 18$, the same conclusion holding for $19 \leq k \leq 24$ where $\rho_c^{(1)} < \rho_s < \rho_c^{(2)}$ [case (c'), not represented here]. In case (d), realized for $k = 25$, some of the metastable states are indeed described by the 1-rsb Ansatz even if the close-packing is frsb.

either $y_c^{(2)} < y_s$ indicating that the close-packing is 1-rsb or $y_c^{(2)} > y_s$ suggesting that it is full rsb. For a given ℓ, we obtain that $y_c^{(2)} < y_s$ at low connectivity ($k \leq k_1$, with $k_1 = 4, 8, 10$ for respectively $\ell = 1, 2, 3$). But things are not exactly that simple since for instance when $\ell = 1$ and $k \geq k_2 = 19$, $y_c^{(2)} < y_s$ again.

5.3 Nature of the close-packing

We now summarize the possible nature of the close-packing by taking into account both kinds of instabilities. Several situations can occur, corresponding to the different relative positions of y_s, the maximum of $\phi(y)$ giving the equilibrium properties with metastable states described by $y < y_s$, $y_c^{(1)}$ indicating an instability of the first kind for $y > y_c^{(1)}$, and $y_c^{(2)}$ indicating an instability of the second kind for $y < y_c^{(2)}$ (note the different directions). All possible combinations seem to be already contained in the $\ell = 1$ model so we will detail it for connectivity ranging from $k = 2$ to $k = 26$; illustrations are provided by Fig. 9 and 10.

Low connectivities $k = 2, 3, 4$ make the best glass models since $y_c^{(2)} < y_s < y_c^{(1)}$, which means that the equilibrium state is 1-rsb and only less dense metastable states are frsb [case (a) of Fig. 10], a behavior similar to p-spin models [26]. When $k = 5$, $y_s < y_c^{(2)} < y_c^{(1)}$ so the equilibrium state is frsb; however there exist some (but not all) untypical graphs with a 1-rsb phase [case (b) of Fig. 10]. When $6 \leq k \leq 24$ the 1-rsb Ansatz is never stable since $y_c^{(1)} < y_c^{(2)}$; however the situation improves somewhat as k increases, with $y_c^{(1)} < y_s < y_c^{(2)}$ for $6 \leq k \leq 18$ ("doubly unstable") and $y_c^{(1)} < y_c^{(2)} < y_s$ ("simply unstable") for $19 \leq k \leq 24$ [case (c) of Fig. 10]. The case $k = 25$ is particularly interesting and justifies our study up to this large connectivity; indeed, we find $y_c^{(2)} < y_c^{(1)} < y_s$, i.e., the equilibrium state is frsb as well as the densest metastable states but there also exist metastable states with intermediate density which are well described by the 1-rsb approach [case (d) of Fig. 10]. Such a strange feature disappears for $k = 26$ (and presumably for all higher k) where we recover the low connectivity situation with $y_c^{(2)} < y_s < y_c^{(1)}$.

6 Dynamical and kinetic transitions

As explained in Sect. 4.8, our lattice glass models undergo a *dynamical transition* at μ_d where the phase space breaks into exponentially many metastable states. Here "dynamical" means that the transition does not affect equilibrium properties, i.e., the grand potential is analytic at μ_d . However, despite its designation, the dynamical transition refers to a *static* property, in the sense that it describes a morphological change of the free energy landscape and makes no reference to a particular kinetic rule. Kinetic transitions (also called "dynamical arrests" [27]) are associated with the freezing of some degrees of freedom of the system under specific local kinetic rules, and form the central concept of kinetically constrained models [2].

We now show that choosing the most natural local dynamical rules leads to several properties: (1) A kinetic

transition at which a finite fraction of particles is blocked takes place beyond a certain chemical potential μ_k. (2) The kinetic freezing at μ_k is a distinct phenomenon from the ergodicity breaking occurring at μ_d. In particular it may happen that $\mu_k < \mu_d$ so that the dynamical transition at μ_d is prevented by a kinetic arrest at μ_k.

The easiest and more natural dynamical rule for our models (the one that, by the way, one can use naturally to simulate it) is the standard Monte Carlo, i.e., at each time step we pick at random a particle on a site i and one of its neighboring site, j, and we move the particle onto j provided that the geometrical constraint remains satisfied after the move (site j has no more than ℓ occupied neighboring site in addition to site i). Furthermore, for simplicity, we focus on the simple $\ell = 1$ model and instead of computing the exact kinetic transition μ_k as done in Ref. [4] for the Kob-Andersen model on the Bethe lattice, we present a simpler calculation consisting in finding the onset of a particular blocked structure. This provides an upper bound $\mu_b > \mu_k$ for the kinetic transition, so that obtaining $\mu_d > \mu_b$ will be enough to prove that $\mu_d > \mu_k$ can occur.

The blocked structure we consider is a percolating structure made of two kinds of blocked particles, either unsaturated or saturated (see Fig. 11). Rooted trees with an unsaturated and saturated blocked particle on the root are associated with the partition functions $\Xi^{(bu)}$ and $\Xi^{(bs)}$ respectively. The relation between the partition functions at different generations g reads

$$\begin{aligned}\Xi^{(bu)}_{g+2} &= e^{\mu} \\ &\left[(\Xi_g)^k - \left(\Xi_g - \Xi^{(b)}_g\right)^k - k\Xi^{(b)}_g \left(\Xi_g - \Xi^{(b)}_g\right)^{k-1}\right]^k \\ \Xi^{(bs)}_{g+3} &= ke^{2\mu} \\ &\left[(\Xi_g)^k - \left(\Xi_g - \Xi^{(b)}_g\right)^k - k\Xi^{(bu)}_g \left(\Xi_g - \Xi^{(b)}_g\right)^{k-1}\right]^k \\ &\left[(g \to g+1)\right]^{k-1}\end{aligned} \tag{105}$$

where $\Xi^{(b)} \equiv \Xi^{(bu)} + \Xi^{(bs)}$, and $\Xi \equiv \Xi^{(e)} + \Xi^{(u)} + \Xi^{(s)}$ is the total partition function (with notations of Sect. 3.1). As illustrated in Fig. 11, the equation for $\Xi^{(bu)}_{g+2}$ includes all configurations at generation g [term $(\Xi_g)^k$] except those where no particle is blocked [$\left(\Xi_g - \Xi^{(b)}_g\right)^k$] and those where only one particle is blocked [$k\Xi^{(b)}_g \left(\Xi_g - \Xi^{(b)}_g\right)^{k-1}$]; in this case, the presence of *two* blocked particles on level g is needed to exclude the possibility that a blocked particle on level g could go at level $g+1$ and then to a different site at level g. The equation for $\Xi^{(bs)}_{g+3}$ has a similar interpretation.

In the liquid phase where the partition functions become independent of the generation g, we can consider the probability for a particle on the root to belong to the blocked structure,

$$p_b \equiv \frac{\Xi^{(b)}}{\Xi^{(u)} + \Xi^{(s)}}. \tag{106}$$

From Eq. (105) and (6-8), it is found to satisfy the self-consistent equation

$$\begin{aligned} p_b = \;& \eta \left[1 - (1-\zeta p_b)^k - k\zeta p_b (1-\zeta p_b)^{k-1}\right]^k \\ &+\theta \Big[1 - (1-\zeta p_b)^k - k\zeta\eta \Big(1 - (1-\zeta p_b)^k \\ &-k\zeta p_b (1-\zeta p_b)^{k-1}\Big)^k (1-\zeta p_b)^{k-1}\Big]^{2k-1} \end{aligned} \tag{107}$$

where ζ, η and θ depend on μ through the relations $\zeta \equiv 1 - e^{-\mu a_{\rm liq}}$, $\eta \equiv (e^{\mu b_{\rm liq}} - 1)/(e^{\mu a_{\rm liq}} - 1)$ and $\theta \equiv (e^{\mu a_{\rm liq}} - e^{\mu b_{\rm liq}})/(e^{\mu a_{\rm liq}} - 1)$. At a given connectivity k we calculate μ_b as the lowest μ such that Eq. (107) has a solution $p_b \in]0, 1]$. For $k \leq 5$ we obtain $\mu_b > \mu_d$, i.e., the blocked structure considered does not appear in the liquid phase. However, for $k = 6$ we find $\mu_b \simeq 1.0$ which is lower than $\mu_d \simeq 2.7$; we can thus conclude for sure that $\mu_k < \mu_d$, i.e., the kinetic freezing occurs while the system is still in its liquid phase.

Let us conclude this section with some remarks on the difference between the dynamical transition obtained from the cavity (or replica) computation and the kinetic freezing that we studied in this section. The kinetic freezing transition is clearly dependent on the dynamics and is related to the fact that after a certain density there are no more paths to go from one part of the configuration space to another. Of course, the allowed paths depend on the local dynamics that has been chosen for the model. If one increases the scale on which particles can move, for example allowing particles jumps on next nearest neighbor or

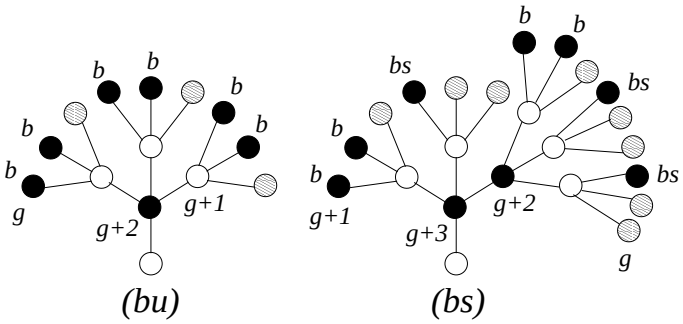

Fig. 11. Illustration of the blocked structure under consideration, with empty sites represented in white, sites occupied by a blocked particle in black and unspecified sites in grey. The structure is made of two kinds of blocked particles. The left figure shows how unsaturated blocked particles (*bu*) at generation $g+2$ are prevented from moving to generation $g+1$ provided sites at generation $g+1$ have at least two blocked neighboring particles b (b meaning either *bu* or *bs*). The right figure shows how saturated blocked particles (*bs*) at generation $g+3$ are similarly blocked by blocked particles at generation $g+1$ and g. In this case a branch can be blocked either by a single *bs* particle, or by two blocked particles.

further, then the density ρ_k, at which the kinetic freezing takes place, is expected to increase. The thermodynamic limit, which does not play an important role for kinetic freezing transitions, is instead very important for the dynamical transitions due to a change of the morphology of the free energy landscape. In the latter case when the number of sites becomes very large some bottlenecks in the configuration space (that has to be used by any local dynamics) shrinks. So, at the end, the configuration space breaks up in different ergodic components.

7 Discussion and conclusions

Some of the qualitative properties of our models such as the presence of a liquid phase at low μ are easily understood. Since our work concerns random graphs with no local disorder, the equilibrium liquid phase is characterized by its homogeneity: the probability that a site is occupied is site-independent. Within the cavity framework, this is reflected by a unique value of the cavity fields which describe in fact probabilities of particle occupation. Due to the tree-like structure of the lattices we consider, such probabilities can be computed recursively. However such an approach is physically justified only if the iterations converge to a unique fixed point regardless of the initial conditions.

When μ is increased, the liquid fixed point becomes unstable and so some kind of equilibrium glassy phase must be present. A clear evidence of the inadequacy of the liquid solution (i.e., of the Bethe-Peierls approximation) is the negative value of the liquid's entropy. In some cases, crystal phases can be constructed and we found these to be thermodynamically favored beyond a melting point μ_m; however such ordered phases occur only on trees with carefully chosen boundary conditions. By focusing on *random graphs*, we exclude this possibility, leaving as the only alternative the existence of an equilibrium glass phase.

The nature of the liquid to glass transition is discontinuous and of the one-step rsb type. This means that the phase space first clusterizes into exponentially many non-ergodic components at some μ_d, before a true equilibrium transition occurs at $\mu_s > \mu_d$. Both transitions are thermodynamical in nature but the transition at μ_d is called a "dynamical transition" to emphasize the fact that equilibrium properties are still given by the liquid solution when $\mu_d < \mu < \mu_s$, and only non-equilibrium properties are affected in this range. More insights into these non-equilibrium effects where obtained by computing the configurational entropy $\Sigma(\omega)$ which gives the number $\mathcal{N}(\omega)$ of (metastable) clusters of configurations with a given grand potential ω, through the relation $\mathcal{N}(\omega) = \exp[N\Sigma(\omega)]$ (with N being the number of sites of the graph).

Investigating the stability of the 1-rsb solution, we found that while the equilibrium configurations may be of 1-rsb type i.e., organized into distinct clusters, some metastable states can be associated with full replica symmetry breaking (frsb), i.e., configurations organized into clusters themselves organized into smaller clusters, and so on. Our study of the $\mu = \infty$ case furthermore demonstrated that, depending on the model, the equilibrium state itself can exhibit frsb, and many different phase space structures are possible.

Finally, we showed that when using standard Monte Carlo dynamical rule a kinetic freezing can occur at $\mu_k < \mu_d$, thus preventing the dynamical transition which is due to a change of the free energy landscape. In a general model, the freezing will therefore occur at $\mu_f = \min(\mu_k, \mu_d)$ and will be of a different nature, purely kinetic or truly thermodynamic, depending on which alternative is realized. The overall picture for lattice glass models given here is quite rich. A natural question is how small loops modify (if at all) this picture; we expect only small quantitative differences. A more fundamental and intriguing issue is therefore what features survive when going to finite dimensional lattices where the large scale Euclidean structure could potentially change even the qualitative aspects.

The last point we would like to emphasize here is that even if our conclusions do not necessarily apply to real vitreous materials, our results should have an impact in optimization problems where random graphs arise naturally. Indeed, as a by-product of our study, we have determined the maximum densities and the phase space structure of different close-packing problems. Our family of models provides a generalization to $\ell \geq 1$ of the hard-core model $\ell = 0$ (called the *vertex cover* problem in computer science and the *largest independent set* problem in the mathematics literature) with, in some cases, 1-rsb features much simpler than the frsb structure of the simplest ($\ell = 0$) hard-core model. A full understanding of these models could therefore constitute a first step toward a mathematical resolution of this fundamental but still unsolved problem [28].

Acknowledgements

We thank Markus Müller for helpful discussions, and in particular for explaining to us the method of Appendix C which he first developed in the context of lattice polymers [29].

Appendix A

In this appendix, we present the generalization of the formulae given for $\ell = 1$ in the core of the paper to an arbitrary $\ell < k$, where ℓ is the maximum number of neighboring particles a given particle can have. It is straightforward to realize that here again, only three degrees of freedom are relevant ($d = 3$) so that we also need only two-component local fields and the situation is very simi-

lar to $\ell = 1$. The recursion relations are now

$$\begin{aligned} a_0 =& \hat{a}(a_1, b_1, \dots, a_k, b_k) \\ =& \frac{1}{\mu} \ln \Big[1 + e^{\mu(1-\sum_{j=1}^{k} a_j)} \\ & \left(1 + \sum_{p=1}^{l} \sum_{1 \le i_1 < \dots < i_p \le k} \prod_{r=1}^{p} (e^{\mu b_{i_r}} - 1) \right) \Big], \end{aligned} \tag{108}$$

$$\begin{aligned} b_0 =& \hat{b}(a_1, b_1, \dots, a_k, b_k) \\ =& \frac{1}{\mu} \ln \Big[1 + e^{\mu(1-\sum_{j=1}^{k} a_j)} \\ & \left(1 + \sum_{p=1}^{l-1} \sum_{1 \le i_1 < \dots < i_p \le k} \prod_{r=1}^{p} (e^{\mu b_{i_r}} - 1) \right) \Big]. \end{aligned} \tag{109}$$

In the $\mu \to \infty$ limit this becomes

$$\begin{aligned} a_0 &= \max \left(0, 1 - \sum_{j=1}^{k} a_j + \max_{1 \le i_1 < \dots < i_l \le k} \sum_{r=1}^{l} b_{i_r} \right), \\ b_0 &= \max \left(0, 1 - \sum_{j=1}^{k} a_j + \max_{1 \le i_1 < \dots < i_{l-1} \le k} \sum_{r=1}^{l-1} b_{i_r} \right). \end{aligned} \tag{110}$$

The Ansatz on integer peaks has exactly the same structure as for $\ell = 1$,

$$\begin{aligned} P(a,b) =& p_e \delta(a)\delta(b) + p_u \delta(a-1)\delta(b-1) \\ & + (1 - p_e - p_u)\delta(a-1)\delta(b) \end{aligned} \tag{111}$$

but of course the relations between the p_a need to be extended:

$$\begin{aligned} p_e &= \frac{1}{Z} \left(1 - \sum_{q=0}^{l} \binom{k}{q} p_u^q p_e^{k-q} \right), \\ p_u &= \frac{1}{Z} \sum_{q=0}^{l-1} \binom{k}{q} p_u^q p_e^{k-q} e^y, \\ Z &= 1 + (e^y - 1) \sum_{q=0}^{l} \binom{k}{q} p_u^q p_e^{k-q}. \end{aligned} \tag{112}$$

Next we can write the corresponding $\phi(y)$ as

$$\begin{aligned} -y\phi(y) =& \ln \left(1 + (e^y - 1) \sum_{q=0}^{l} \binom{k+1}{q} p_1^q p_0^{k+1-q} \right) \\ & - \frac{k+1}{2} \ln \left(1 + (e^{-y} - 1)[(1-p_0)^2 - p_1^2] \right). \end{aligned} \tag{113}$$

The study of the stability follows the same principle as for $\ell = 1$, the only difficulty being to correctly collect all the combinatorial factors. The matrix for the instability of the second kind is

$$T = \begin{bmatrix} 0 & 0 & 0 & 0 & t_{01,20} & t_{01,21} \\ 0 & 0 & t_{02,10} & 0 & t_{02,20} & t_{02,21} \\ 0 & t_{10,02} & 0 & t_{10,12} & 0 & 0 \\ t_{12,01} & 0 & 0 & 0 & 0 & 0 \\ (k-l)e^{-y_2} & (k-l)e^{-y_2} & 0 & le^{-y_2} & 0 & 0 \\ 0 & 0 & l & 0 & 0 & 0 \end{bmatrix} \tag{114}$$

with

$$\begin{aligned} t_{01,20} &= \frac{1}{Z} \sum_{q=0}^{l-1} k \binom{k-1}{q} p_e^{k-q-2} p_u^q p_s e^y, \\ t_{01,21} &= \frac{1}{Z} \sum_{q=0}^{l-1} k \binom{k-1}{q-1} p_e^{k-q-1} p_u^{q-1} p_s e^y, \\ t_{02,10} &= \frac{1}{Z} (l+1) \binom{k}{l+1} p_e^{k-l-2} p_u^{l+1} e^y, \\ t_{02,20} &= \frac{1}{Z} k \binom{k-1}{l} p_e^{k-l-2} p_u^l p_s e^y, \\ t_{02,21} &= \frac{1}{Z} k \binom{k-1}{l-1} p_e^{k-l-1} p_u^{l-1} p_s e^y, \\ t_{10,02} &= \frac{1}{Z} \sum_{q=0}^{l-1} (k-q) \binom{k}{q} p_e^{k-q} p_u^{q-1}, \\ t_{10,12} &= \frac{1}{Z} \sum_{q=0}^{l-1} q \binom{k}{q} p_e^{k-q} p_u^{q-1}, \\ t_{12,01} &= \frac{1}{Z} l \binom{k}{l} p_e^{k-l+1} p_u^{l-2} e^y, \end{aligned} \tag{115}$$

where $p_s \equiv 1 - p_e - p_u$ and $Z = 1 + (e^{y_1} - 1) \sum_{q=0}^{l} \binom{k}{q} p_u^q p_e^{k-q}$.

Appendix B

In this appendix we shall show how the stability criterion at $\mu = \infty$ derived in the text can be obtained within a response function formalism.

First let us note that as far as the fragmentation of the cluster is concerned we can merely take the $\mu = \infty$ of the formalism introduced in Sect. 4.9. Indeed in the close-packing limit there is a total freezing within each state. Hence, it is relatively easy to obtain the correlation length ζ_2. The computation of $\overline{\langle n_i n_j \rangle}$ can be done using the transfer matrix:

$$T_{A,B} = \sum_{(A, a_2 \dots, a_k) \to B} p_{a_2} \dots p_{a_k} \exp[-y \Delta E_{(A, a_2, \dots, a_k)}], \tag{116}$$

$$\overline{\langle n_0 n_r \rangle} = \frac{P_0^t T^r P_0'}{P_*^t T^r P_*'} \tag{117}$$

where P_0^t and P_0' are suitable vectors to impose that there is a particle in 0 and r. The other vectors P_*^t and P_*' read with the bracket notation:

$$\langle P_* | a \rangle = p_a, \qquad \langle a | P_*' \rangle = \sum_{b \text{ compatible with } a} p_b. \tag{118}$$

What is important to notice is that they are respectively the left and right eigenvectors of T with largest eigenvalues, Z, in module. The properties of being eigenvectors can be checked but it is fundamentally due to the fact that p_a is the self-consistent solution of the iterative cavity equations which can be written going from left to right or from right to left on the 1D chain. The fact that they correspond to the largest eigenvalue in module is just due to the Perron-Frobenius theorem (T is irreducible with positive coefficient and the two eigenvectors have all the components with the same sign).

Generically T can be written in terms of its right and left eigenvectors:

$$T = \sum_\alpha \Lambda_\alpha |v_\alpha >< w_\alpha|, \qquad < w_\beta | v_\alpha >= \delta_{\alpha,\beta}, \quad (119)$$

where the $\alpha = 1$ corresponds to P^t_*, P'_* (note however that P^t_* and P'_* are not normalized between one another) and $\Lambda_1 = Z$.

Plugging this expression into the equations for the correlation function one obtains generically that the correlation function reads:

$$\overline{\langle n_0 n_r \rangle} = C + \sum_{i=2}^{d} D_i \left(\frac{\Lambda_i}{\Lambda_1} \right)^r \quad (120)$$

where C and D_i are constants that can be expressed in terms of the scalar product of the eigenvectors. In particular it can be shown that $C = \rho^2$ as it should. Thus, the stability with respect to fragmentation of the cluster is governed by the condition $k \left(\frac{|\Lambda_2|}{\Lambda_1} \right)^2 < 1$.

Finally, we want to show that this condition is the same as the one given in Sect. 5.2.2. Let us define the matrix $\tilde{T}$:

$$\tilde{T}_{A,B} = \frac{1}{Z} \left(T_{A,B} - p_B \sum_C T_{A,C} \right) \quad (121)$$

This matrix has eigenvalues:$0, \frac{\Lambda_2}{\Lambda_1}, \ldots, \frac{\Lambda_n}{\Lambda_1}$. One can check this in different ways. For example $\mathrm{Tr}\tilde{T}^l = \sum_{i=2}^n \left(\frac{\Lambda_i}{\Lambda_1} \right)^l$ for any l, so the eigenvalues are indeed the ones predicted. In terms of $\tilde{T}$ the stability criterion is that k times the square of the largest eigenvalue of $\tilde{T}$ has to be less than one. This is exactly the criterion obtained in the text by studying the stability of the iterative Eq. (86) for the 1-rsb glass (where the normalization Z is considered as a function of the p_a).

The second instability, the fragmentation of states, cannot be obtained taking simply the $\mu \to \infty$ limit of the formalism described in Sect. 4.9. Because of the complete freezing within a state in the close packing limit the connected correlation functions are trivially zero. This, of course, does not mean that there is no way to identify a correlation length. Actually, one has just to resort to a definition of correlation length in terms of response functions. Let us remark that the correlation function $\langle n_0 n_r \rangle_c$ can be written as:

$$p_0^o p_0^e \left(\langle n_r \rangle_o - \langle n_r \rangle_e \right) \quad (122)$$

where p_0^o and p_0^e are respectively the probability that the site 0 is occupied or empty and the averages $\langle \cdot \rangle_o$ and $\langle \cdot \rangle_e$ are the averages conditioned on the events $n_0 = 1$ or $n_0 = 0$. At finite μ computing $\langle n_0 n_r \rangle_c$ or the response function $(\langle n_r \rangle_o - \langle n_r \rangle_e)$ contains the same amount of information as far as the correlation length is concerned. However at infinite μ there is total freezing within a state. As a consequence the product $p_0^o p_0^e$ equals zero and one is forced to extract the correlation length from the response functions. Thus one has to study the change in probability for the occupation variable at site r when the value of occupation variable in 0 is changed. This gives rise naturally to the eigenvalue problem discussed in Section 5.2.3. In that case the matrix entering in the eigenvalue problem tell us how the effect of replacing a with e by changing only one parent propagates from a site to its neighbor.

Appendix C

We present here on the specific case of the lattice glass with $\ell = 1$ how Eq. (104) allows for a straightforward study of the 1-rsb stability. We start with the composition rules Eq. (89). With the notations of this section, we have $d = 3$ and the configurations are $a \in \{e, u, s\}$. Let us see for instance how the matrix elements corresponding to $\lambda_{s \to e}$ are computed. We have to ask how the configuration of one parent on the left hand-side of

$$u + e + \cdots + e \to s \quad (123)$$

must be changed if we want to obtain a configuration e instead of s. Begin with the parent u: according to the composition rules, if we replace it by e it leads to a child u so we do not retain this possibility; instead, if we replace it by s we indeed obtain e. If we now keep u but try to "flip" one of the e's, we see that both replacements by u or s lead to a child e as we wish. So we have a total of three cases to take into account, a situation that we summarize by writing the following "reaction" rules:

$$\begin{aligned} (e|s) &\leftarrow (s|u) + \underbrace{e + \cdots + e}_{k-1}, \\ (e|s) &\leftarrow u + (u|e) + \underbrace{e + \cdots + e}_{k-2}, \\ (e|s) &\leftarrow u + (s|e) + \underbrace{e + \cdots + e}_{k-2}. \end{aligned} \quad (124)$$

Now recall that the initial "reaction" formula (123) represents in fact the equation

$$p_s = Z^{-1} k p_u p_e^{k-1} e^y \quad (125)$$

where Z is a normalization constant, $k p_u p_e^{k-1}$ is the probability to choose parents $(u, e, \ldots, e)$ when each configuration a is taken with its probability p_a, and the reweighting term e^y is added each time the generated child is u or s, i.e., corresponds to a new particle. Generalizing slightly

the same principle, just by looking at the reaction equations (124), we write

$$\begin{aligned} p(e|s) =& Z^{-1}kp(s|u)p_e^{k-1} + Z^{-1}k(k-1)p_u p(u|e)p_e^{k-2} \\ &+ Z^{-1}k(k-1)p_u p(s|e)p_e^{k-2}. \end{aligned} \tag{126}$$

Here we put no reweighting since we generate an empty site e. Using the equations for the p_a, it can be simplified somewhat, and when expressed with the $\lambda_{a\to e}$ defined by $p(e|a) \equiv p_a \lambda_{a\to e}$, it becomes

$$\lambda_{s\to e} = [\lambda_{u\to s} + (k-1)\lambda_{e\to u} + (k-1)\lambda_{e\to s}]e^{-y}. \tag{127}$$

The five other equations are obtained by following the same lines,

$$\begin{aligned} \lambda_{u\to e} =& k\lambda_{e\to s}e^{-y}, \\ \lambda_{u\to s} =& k\lambda_{e\to u}, \\ \lambda_{s\to u} =& \lambda_{u\to e}, \\ \lambda_{e\to u} =& Z^{-1}kp_s p_e^{k-2}\lambda_{s\to e}e^{y}, \\ \lambda_{e\to s} =& Z^{-1}kp_s p_e^{k-2}\lambda_{s\to u}e^{y} + Z^{-1}k(k-1)p_u^2 p_e^{k-3}\lambda_{u\to e}e^{y} \\ &+ Z^{-1}k(k-1)p_u p_s p_e^{k-3}\lambda_{s\to e}e^{y}. \end{aligned} \tag{128}$$

These six linear relations define the matrix T; we then compute its eigenvalue Λ_2 as a function of y.

Appendix D

In this appendix we would like to show how the results obtained in the text with the cavity method can be reproduced with replicas. For an introduction to the replica method for random graphs with finite connectivity see for example [30].

First, we introduce a function to encode in a compact way the conditional probability that the central site i for a rooted sub-tree is empty (e), occupied but the constraint unsaturated (u) and finally occupied and the constraint saturated (s), i.e., the root site has ℓ neighboring particles. We use the function $f(\tau) = C\exp(h\tau + g\tau^2)$ with $\tau = -1, 0, 1$ where C, h, g are defined in such a way that

$$\begin{aligned} f(0) &= \frac{\Xi_i^{(e)}}{\Xi_i^{(e)} + \Xi_i^{(u)} + \Xi_i^{(s)}}, \\ f(1) &= \frac{\Xi_i^{(s)}}{\Xi_i^{(e)} + \Xi_i^{(u)} + \Xi_i^{(s)}}, \\ f(-1) &= 1 - f(0) - f(1) = \frac{\Xi_i^{(u)}}{\Xi_i^{(e)} + \Xi_i^{(u)} + \Xi_i^{(s)}}. \end{aligned} \tag{129}$$

The relation with the fields a, b can be easily established:

$$\exp(-\mu a) = \frac{1}{1 + \exp(g-h) + \exp(g+h)}, \tag{130}$$

$$\exp(-\mu b) = \frac{1}{1 + \exp(g-h)}. \tag{131}$$

Now consider n replicated systems for the same random graph and define the function $\psi(\boldsymbol{\tau})$:

$$\psi(\boldsymbol{\tau}) = \mathcal{N} \overline{< \prod_{a=1}^{n} \exp(h_i^{(a)}\tau_a + g_i^{(a)}\tau_a^2) >} \tag{132}$$

where the overline means the average over the disorder (or, analogously, one can average over sites for a fixed random graph), $\mathcal{N}$ is a normalization constant such that $\sum_{\boldsymbol{\tau}} \psi(\boldsymbol{\tau}) = 1$ and $\boldsymbol{\tau} \equiv (\tau_1, \dots, \tau_n)$.

For the same reasons as discussed in the text in the case of the cavity method, the grand potential per site is given by:

$$2\omega = \lim_{n\to 0} \frac{1}{n} \left(-(k+1)G_{\text{edge}}^{(n)} + 2G_{\text{site}}^{(n)} \right), \tag{133}$$

$$G_{\text{edge}}^{(n)} = \ln \sum_{\boldsymbol{\tau},\boldsymbol{\tau'}} \psi(\boldsymbol{\tau})\psi(\boldsymbol{\tau'})C(\boldsymbol{\tau},\boldsymbol{\tau'}), \tag{134}$$

$$G_{\text{site}}^{(n)} = \ln \sum_{\boldsymbol{\tau_i},\boldsymbol{n_o}} \prod_{i=1}^{k+1} \psi(\boldsymbol{\tau_i})C(\{\boldsymbol{\tau_i}\},\boldsymbol{n_0}) \tag{135}$$

where $C(\boldsymbol{\tau},\boldsymbol{\tau'})$ and $C(\{\boldsymbol{\tau_i}\},\boldsymbol{n_0})$ enforce the geometrical constraint.

Differentiating ω with respect to $\psi(\boldsymbol{\tau})$ we get the self-consistent equation

$$\psi(\boldsymbol{\tau}) = \mathcal{N} \sum_{\boldsymbol{n_0},\boldsymbol{\tau_i}}{}' \prod_{i=1}^{k} \psi(\boldsymbol{\tau_i})C(\{\boldsymbol{\tau_i}\},\boldsymbol{n_0}) \tag{136}$$

where the prime over Σ means that, for each value of $\boldsymbol{\tau}$, we sum only over those $\boldsymbol{\tau_i}, \boldsymbol{n_0}$ that give rise to $\boldsymbol{\tau}$.

Once the distribution $\psi(\boldsymbol{\tau})$ is known all the observables can be computed. For instance the density equals:

$$\rho = \lim_{n\to 0} \frac{1}{n} \sum_{a,\boldsymbol{\tau_i},\boldsymbol{n_o}} n_o^a \prod_{i=1}^{k+1} \psi(\boldsymbol{\tau_i})C(\{\boldsymbol{\tau_i}\},\boldsymbol{n_0}) \tag{137}$$

The most general replica symmetric solution can be written:

$$\psi(\boldsymbol{\tau}) = \int dhdgP(h,g) \prod_{a=1}^{n} \frac{\exp(h\tau_a + g\tau_a^2)}{1 + \exp(g+h) + \exp(g-h)} \tag{138}$$

where P is a normalized probability distribution. Because of the homogeneity of the random graph with fixed connectivity, the rs solution is particularly simple,

$$P(h,g) = \delta(h - h_{\text{liq}})\delta(g - g_{\text{liq}}). \tag{139}$$

Using the relations (130-131) between h, g and a, b one can rederive all the liquid properties (density, free energy, entropy, ...) obtained in the main part of the paper with the cavity method.

Because of the homogeneity of the random graph, the 1-rsb solution, in which replicas are divided in n/m groups

(noted c) of m replicas each, also becomes simple and reads

$$\psi(\boldsymbol{\tau}) = \prod_{c=1}^{n/m} \int dh dg P(h,g) \frac{\exp[\sum_{a\in c}(h\tau_a + g\tau_a^2)]}{[1+\exp(g+h)+\exp(g-h)]^m}. \quad (140)$$

Plugging this expression into the general equation for $\psi(\boldsymbol{\tau})$ and changing variables from h, g to a, b we get back to the equation on $P(a,b)$, Eq. (43). Moreover using this 1-rsb expression of $\psi(\boldsymbol{\tau})$ one can easily obtain all the observables like the density, the free energy and the complexity.

References

1. L. C. E. Struik, *Physical aging in amorphous polymers and other materials.* (Elsevier, Houston, 1978).
2. F. Ritort and P. Sollich, Adv. Phys. **52**, 219 (2003).
3. W. Kob and H. A. Andersen, Phys. Rev. E **48**, 4364 (1993).
4. C. Toninelli, G. Biroli, and D. S. Fisher, (2003), cond-mat/0306746.
5. G. Biroli and M. Mézard, Phys. Rev. Lett. **88**, 025501 (2002).
6. M. P. Ciamarra, M. Tarzia, A. de Candia, and A. Coniglio, Phys. Rev. E **67**, 057105 (2003).
7. M. Weigt and A. K. Hartmann, Europhys. Lett. **62**, 533 (2003).
8. T. C. Hales, (1998), available at http://www.math.pitt.edu/∼thales/PUBLICATIONS/.
9. G. Szipiro, Nature **424**, 12 (2003).
10. T. Kirkpatrick and D. Thirumalai, Phys. Rev. Lett. **58**, 2091 (1987).
11. T. Kirkpatrick and D. Thirumalai, Phys. Rev. B **36**, 5388 (1987).
12. T. Kirkpatrick, D. Thirumalai, and P. Wolynes, Phys. Rev. A **40**, 1045 (1989).
13. T. Kirkpatrick and P. Wolynes, Phys. Rev. A **35**, 3072 (1987).
14. M. Mézard, G. Parisi, and M. A. Virasoro, *Spin-Glass Theory and Beyond*, Vol. 9 of *Lecture Notes in Physics* (World Scientific, Singapore, 1987).
15. J.-P. Bouchaud, L. Cugliandolo, J. Kurchan, and M. Mézard, in *Spin Glasses and Random Fields*, edited by A. P. Young (World Scientific, Singapore, 1998).
16. M. Mézard, G. Parisi, and R. Zecchina, Science **297**, 812 (2002).
17. L. K. Runnels, J. Math. Phys. **8**, 2081 (1967).
18. R. J. Baxter, Annals of Combin. **3**, 191 (1999).
19. M. Weigt and A. K. Hartmann, Phys. Rev. E **63**, 056127 (2001).
20. M. Mézard and G. Parisi, Eur. Phys. J. B **20**, 217 (2001).
21. F. R. Kschischang, B. Frey, and H.-A. Loeliger, IEEE Trans. Inform. Theory **47**, 498 (2001).
22. J. S. Yedidia, W. F. Freeman, and Y. Weiss, technical report TR-2002-35, Mitsubishi Electrical Research Laboratories (2002), available at http://www.merl.com.
23. R. Monasson, Phys. Rev. Lett. **75**, 2847 (1995).
24. M. Mézard and G. Parisi, J. Stat. Phys. **111**, 1 (2003).
25. S. Franz and M. Leone, J. Stat. Phys. **3-4**, 535 (2003).
26. A. Montanari and F. Ricci-Tersenghi, Eur. Phys. J. B **33**, 339 (2003).
27. A. Lawlor *et al.*, Phys. Rev. Lett. **89**, 245503 (2002).
28. D. Aldous and M. Steele, in *Encyclopedia of Mathematical Sciences*, edited by H. Kesten (Springer, ADDRESS, 2003), Vol. 110, pp. 1–72.
29. A. Montanari, M. Müller, and M. Mézard, (2003), cond-mat/0307040.
30. R. Monasson, J. Phys. A **31**, 515 (1998).